Frequency Domain Modelling of a Coupled System of Floating Structure and Mooring Lines: an application to a Wave Energy Converter

Imanol Touzon[1,3], Vincenzo Nava[2,4], Zhen Gao[5], Victor Petuya[3]

[1] IDOM Engineering, Consulting and Architecture S.A.U., Av. Zarandoa 23, 48015 Bilbao, Spain
[2] Tecnalia, Basque Research and Technology Alliance (BRTA), Edificio 700, 48160, Derio, Bizkaia, Spain
[3] Department of Mechanical Engineering, University of the Basque Country - UPV/EHU, Spain
[4] Basque Centre for Applied Mathematics, BCAM, Bilbao, Spain
[5] Department of Marine Technology, Norwegian University of Science and Technology - NTNU, Norway

Abstract

Floating structures for single offshore renewable energy devices, i.e. wave energy converters, tend to be significantly smaller than those of the traditional offshore industry and the interaction between floater motions and mooring line dynamics become important. Installation sites are generally subject to powerful waves and currents experiencing more dynamically excited motions. Water depths are also lower, ranging generally from 50m to 200m and mooring systems are to be designed to assure the station keeping of them while not interfering with the power conversion. However, floater motions may induce large dynamic tensions on mooring lines, making quasistatic analyses inaccurate in terms of design tension while non-linear time domain simulations too time consuming. This paper introduces a numerical model of lumped mass for mooring lines and rigid body motions for the floating structure coupled by means of kinematic relations, and its subsequent linearization, which is solved in the frequency domain. The linearized model is applied to a two-body floating spar type oscillating water column, subject to the 36 most occurrent sea states at the BIMEP site. Its accuracy is verified through a comparison with the equivalent time domain simulation and a review of the results and its limitations are also pointed out.

Keywords

Frequency Domain; Catenary Mooring System; Linear Hydrodynamics; Lumped mass; Oscillating Water Column; Offshore Renewable Energy

1 Introduction

Mooring systems are very nonlinear mechanical systems and have traditionally been simulated with nonlinear time domain (TD) numerical models, based on either the lumped mass or the finite element method (FEM). Non linearities present in such models arise mainly from the nonlinear geometric stiffness and lines' drag and inertia forces. Both methods are widely used in the offshore industry since initially introduced by [1], and have been applied within the offshore renewable energy sector by [2] and [3], among others, showing accurate results and highlighting the poor tension estimation of the quasistatic (QS) approach. Nevertheless, the

required computation time of the lumped mass method tends to be significant compared with the frequency domain (FD) analysis. Several models have been proposed to account for the mooring influence on the floating structure in the offshore industry in general and in the wave energy conversion sector. An initial approach can be the linearization of the nonlinear geometric stiffness at the mean horizontal position of the structure as suggested in [4]. Through this procedure main horizontal motions are acceptably reproduced whilst just the order of magnitude of line tensions can be estimated, as pointed out in [5] for a wave energy converter (WEC). Other authors, e.g. [6] and [7], added an equivalent impedance to the floater linear hydrodynamics to include the influence of mooring lines and assess the impact on wave energy extraction. Larsen and Sandvik [8] proposed two models, one based on the catenary equations and an estimate of the line drag resistance and a second one based on a model of a single degree of freedom (dof) per line. The additional dof of the latter model consisted of a mode with the shape of the static line with the top end moving in the tangential direction, deriving a transfer function that relates the top end motion with the line tension. They found good agreement with the second model for a wide range of mooring configurations. A method to estimate both floater and lines' dynamic tensions in both FD and TD was introduced in [9] for structures moored in ultradeep waters. It consists in building up the mass, stiffness and damping matrices to represent lines structural properties, coupled with the floater motions and linearizing for the viscous drag term. Lines' motion results are postprocessed so that the line tensions can be derived. In addition, the same authors suggested a hybrid TD and FD methods [10] for intermediate water depths, i.e. 200m, as the geometric non-linear stiffness is more relevant in lower water depths, showing accurate results. A frequency domain solution compared to the corresponding time domain solution of an spar floating platform was also presented in [11]. It was applied to a large spar platform compared with a WEC in deep waters (760m). Good results were obtained, pointing out that most differences may have been produced by the viscous drag force linearization.

The present paper extends the method in the FD introduced by [9], complementing it with a linearized stiffness matrix, to account for the geometric stiffness influence also on mooring lines. The extended methodology for coupled response analysis in the FD is introduced in the first section of the paper, which can be applied to any moored floating structure. Its accuracy is illustrated by comparing its results with the equivalent TD non-linear model of a two-body spar type oscillating water column (OWC) WEC, in operational conditions. Most WECs extract power from incoming waves as the floater is excited and moves, mostly in heave or pitch, in or near resonance with respect to the surface water level (SWL). There are currently some relevant WEC developments close to the precommercial phase such as the Ocean Energy buoy [12], the MARMOK OWC [13] or the CorPower heaving buoy [14], all based on the energy captured in their oscillating motions.

Specifically, OWCs consist of a structure, either floating or seabed mounted, and an internal water column, connected with the sea water at the bottom and with an air chamber at the top. The power is extracted from the pressure of the air chamber, induced by relative motion of the structure with respect to the internal water surface. The compressed and expanded air is made to pass through a self-rectifying air turbine allocated on the deck of the floating structure. Its hydrodynamic properties for power production assessment can be

modelled, among other methods, through two oscillating bodies, one representing the floater and a second one, consisting of a massless surface on the internal SWL, representing the free surface water of the internal water column. The case study considered here is a floating spar type OWC, which extracts wave power from the heaving relative motions between the floater and the internal water column, intensively studied in [15], [16]. It has been assumed a catenary spread mooring system made up of three lines is used for the station keeping of the floating WEC. It is a very commonly used mooring system, in which the above-mentioned nonlinearities play a key role in its performance, i.e. the geometric stiffness, drag and inertia forces and the interaction with the seabed.

Floater motions are calculated with hydrodynamic coefficients, obtained with a commercial code [17] based on the linear potential flow theory, and including additional viscous drag forces and second order wave drift forces. Mooring line motions are based on the non-linear lumped mass method and are coupled to the floater by kinematic relations. The non-linear floater and mooring system coupled model has been validated with tank test results, and introduced in [18]. In the present work all non-linear effects, such as drag force on the floater and line sections as well as the geometric stiffness, have been linearized through statistical linearization for random waves. In addition, non-linear kinematic relations have been linearized at the mean position, enabling the resolution of the coupled mechanical system in the FD.

The motions and line tensions obtained with the linearized system are presented and compared with the equivalent non-linear TD model for the most occurrent sea states at BiMEP site, described in [19].The accuracy of line tension results along mooring lines, from the fairlead to the anchor have also been compared obtaining good agreement, especially in the fairleads. Finally, some limitations of the current approach have been explained, supported by the modal analysis of the coupled system.

2 Numerical models

2.1 Time domain numerical model

The floater and mooring coupled non-linear TD numerical model, used as the reference model in this work, has been introduced and validated in [18]. Motions of several diffracting bodies can be included to represent WECs, mostly made up of more than one diffracting body. The wave structure interaction numerical model of the floater is based on the linear potential flow theory and Boundary Integral Element Method (BIEM). The applied commercial code [17] provides linear hydrodynamic coefficients, assuming small wave amplitudes compared to the wavelength. This assumption leads to linearized kinematic and dynamic free surface boundary conditions [20]. The mooring model is based on the lumped mass method, which accounts for the non-linear geometric stiffness as well as the drag and inertia forces on mooring lines, relevant effects in line tension estimates. The model makes use of Lagrange multipliers through the penalty method [21] to account for all kinematic relations. On the one hand kinematic constraints can be set between the diffracting bodies, e.g. the floating structure and the internal water surface, that, along with the power take off (PTO) force, represent the

floating WEC. On the other hand, the fairlead and anchor points of the mooring lines are imposed to be attached to the fairleads in the floating structure and fixed on the seabed respectively. The complete numerical model is represented in the TD, in equation (1), accounting for both radiation, hydrostatic, wave, inertia and anchoring forces, in which the main non-linearities arise from the seabed, viscous drag and catenary geometric stiffness forces. Therefore, in equation (1) the first set of degrees of freedom represent the floating structure (*'str'*) along with its kinematic relations (*'dkin'*), in case of a floater made up of multiple diffracting bodies. The last set of degrees of freedom represent the nodes of all mooring lines (*'moor'*) describing the lumped mass method.

$$\begin{bmatrix} (M+A)_{str}+M_{dkin} & M_{f/a} \\ M_{f/a} & M_{moor} \end{bmatrix} \cdot \begin{Bmatrix} \ddot{\delta}_{str}(t) \\ \ddot{\delta}_{moor}(t) \end{Bmatrix} + \begin{bmatrix} C_{pto}+C_{dkin} & C_{f/a} \\ C_{f/a} & C_{moor} \end{bmatrix} \cdot \begin{Bmatrix} \dot{\delta}_{str}(t) \\ \dot{\delta}_{moor}(t) \end{Bmatrix} + \begin{bmatrix} H_{str}+K_{pto}+K_{dkin} & K_{f/a} \\ K_{f/a} & K_{moor} \end{bmatrix} \cdot \begin{Bmatrix} \delta_{str}(t) \\ \delta_{moor}(t) \end{Bmatrix} = \begin{Bmatrix} F_w(t)+F_{sv}(t)+F_{drag}(t)-F_{rad}(t)-F_{f/a}^{qs}(t) \\ F_z(t)+F_f(t)+F_g+F_b+F_{morison}(t)+F_{f/a}^{qs}(t) \end{Bmatrix} \quad (1)$$

In equation (1) the subscript *'str'* denotes floating structure, *'moor'* denotes mooring, *'pto'* denotes power take off, *'dkin'* denotes kinematic relations between diffracting bodies and *'f/a'* denotes fairlead and anchor forces. In addition, the intervening variables are:

- *M, C, K*: Mass, damping and stiffness matrices of the corresponding 'subsystem'
- *A, H*: Infinite-frequency added mass and hydrostatic matrices
- $F_w, F_{sv}, F_{drag}, F_{rad}, F_{f/a}^{qs}$: Froude-Krilov and diffraction, slowly varying second order drift, viscous drag, radiation and fairlead forces on the floater
- $F_z, F_f, F_g, F_b, F_{morison}, F_{f/a}^{qs}$: Seabed vertical reaction, seabed horizontal friction, gravity, buoyancy, Morison and fairlead-anchor forces on mooring lines
- $\delta(t), \dot{\delta}(t), \ddot{\delta}(t)$: Floating structure rigid body and mooring lumped masses position, velocity and acceleration. Six dof per floating structure and multiple dof-s for mooring lines, based on the lumped mass model

It should be noted that the force to impose mooring lines upper ends to follow the fairleads in the floating structure is composed of two main terms. The variable forces arisen from $M_{f/a}$, , $C_{f/a}$ and $K_{f/a}$ and the quasistatic forces $F_{f/a}^{qs}$. The former make the fairleads to move with the centre of gravity of the floating structure while the latter, $F_{f/a}^{qs}$, stands for the forces to maintain fairleads at a constant position from the centre of gravity of the floating structure, as well as keeping anchors fixed in the corresponding seabed positions.

The magnitude of $F_{f/a}^{qs}$ depends on the positions of the fairlead and anchor points with respect to the centre of gravity of the floater at each time step, $\delta_{x,y,z-fair}$ and $\delta_{x,y,z-anchor}$ respectively in equation (12). Whilst $\delta_{x,y,z-fair}$ is time invariant in the floater-fixed coordinate system, $\delta_{x,y,z-anchor}$ changes along the time as the floater moves, and the corresponding force, built up as a constant force in (13) with the restrictions set in (12), needs to be updated every time step. Fairleads and anchors quasistatic force component, $F_{f/a}^{qs}$, on the floating structure corresponds to the forces of all lines attached to the floating structure and with opposite sign with

respect to the $F_{f/a}^{qs}$ on the corresponding attachment nodes on mooring lines. However, as the force is not proportional to any dof, it does not intervene in the linearized system introduced in equation (15). All kinematic restrictions on mooring line ends (blue triangles) are represented in Figure 1.

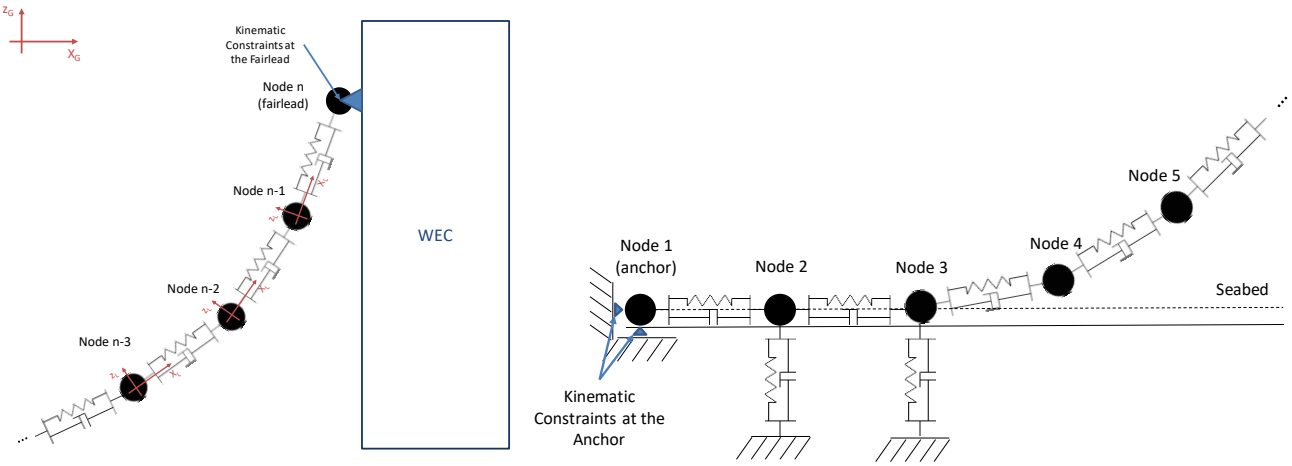

Figure 1. Mooring line schematic representation. Last four nodes and the fairlead with local and global coordinates (top) and first five nodes and the anchor (bottom). The kinematic constraints to maintain the anchor and fairleads are represented with blue triangles, each node is represented as a concentrated mass linked to adjacent nodes by spring and dampers, representing the lines axial properties. The seabed is also represented by stiffness and dampers and the node numbering is increased from the anchor to the fairlead.

The lumped mass method consists in discretizing mooring lines in a set of point masses, with a mass equivalent to the sum of half the mass of its adjacent segments. Each point mass is linked to its adjacent point masses through linear and, if bending is considered, rotational spring and dampers of equivalent properties to the actual line to be modelled. These elements have been represented in Figure 1 along with the global and local coordinate systems. The global coordinate system (G) is assumed to be on the sea SWL, with the positive 'Z_G' axis pointing upwards. In addition to the internal forces, the external forces, such as hydrodynamic Morison force, seabed, buoyancy and gravity forces are also included. The change in the line shape with small motions of the floater makes it a significantly non-linear system, being necessary to update the internal forces every time step.

The dynamic system described in equation (1) is composed of three main parts, the floater, mooring lines and the lines fairleads and anchor. All of them have been included in the numerical model through sets of stiffness, damping and mass matrices or as time varying forces. Floater motions are linear since its wave structure interaction have been computed with a linear potential code and, hence, its matrices are time invariant. The PTO force has been modelled as a set of linear stiffness and damping matrices, acting between the heaving motions of the internal SWL and the floater. It represents the air turbine influence in the case study of the OWC here introduced, which can be modelled as a linear force in case a Wells turbine is used [22]. The radiation force F_{rad} in the TD is computed by a convolution of the radiation impulse response function and the velocity of the corresponding degree of freedom. There are several methods proposed to perform it, most of them based in state space models and used in several codes presented in [23], however, in this work the radiation force has been computed through direct integration of the convolution of the retardation function and the corresponding velocity history at each time step.

In the non-linear TD model represented in equation (1) several non-linear terms are found. One of the major sources of nonlinearities in offshore structures is the viscous force, represented by the last term in the right hand side (RHS) of equation (2), which also applies to the mooring lines.

$$F_{morison}(t) = (1 + C_a) \cdot \rho_w \cdot V \cdot \dot{u}(t) - C_a \cdot \rho_w \cdot V \cdot \ddot{\delta}(t) + 0{,}5 \cdot \rho_w \cdot C_d \cdot D \cdot L \cdot \left|u(t) - \dot{\delta}(t)\right| \cdot \left(u(t) - \dot{\delta}(t)\right) \quad (2)$$

Where:

- $C_a \; and \; C_d$: Added mass and drag coefficients respectively
- ρ_w: Water density
- $V, D \; and$ L: Volume of the equivalent line length, line equivalent diameter and the line length associated to the corresponding point
- u(t): water particle velocities

The slowly varying (SV) wave drift forces are also non-linear forces [24]. These forces are computed for each pair of frequencies and the product of the corresponding amplitudes over a double summation, as shown in (3).

$$F_{sv}{}^{i}(t) = \sum_{j=1}^{N}\sum_{k=1}^{N} A_j \cdot A_k \cdot \left[T_{jk}^{ic} \cdot cos\{(\omega_k - \omega_j) \cdot t + (\varphi_k - \varphi_j)\} + T_{jk}^{is} \cdot sin\{(\omega_k - \omega_j) \cdot t + (\varphi_k - \varphi_j)\}\right] \quad (3)$$

In (3) each frequency is denoted through 'j' and 'k' respectively, wave amplitudes through A, frequencies with ω, phases with φ and degrees of freedom with 'i'. The variable 'T' indicates the quadratic transfer function (QTF), computed here with the Newman approximation [24]. The main diagonal of the QTF has been obtained with a linear potential flow code [17]. Only the horizontal $F_{sv}{}^{1}(t)$ has been considered in both models. The first order wave excitation forces have been computed with the linear Froude-Krylov and diffraction force per unit amplitude ($\hat{F}_{w-R.A.O.}(\omega)$), obtained with the linear potential flow solver [17]. Such excitation forces have been computed in the TD through the ifft of the corresponding force amplitude, $F_w(t) = \sum_{k=1}^{N} \hat{F}_{w-R.A.O.}(\omega_k) \cdot A_k(\omega_k) \cdot e^{i\cdot(\omega_k \cdot t + \varphi_k)}$. The term φ_k denotes the wave phase, taken as uniformly distributed random numbers in the range $0 < \varphi_k < 2 \cdot \pi$.

The mooring system is fully non-linear since its stiffness and damping matrices are time variant to account for the geometric changes. Its interaction with the seabed, is also non-linear as it just acts vertically upwards in the case of the vertical reaction, whilst the horizontal friction force is limited in magnitude to the absolute friction force. The gravity force on mooring lines is the responsible for the geometric non-linear stiffness as its influence on the lifted sections from the seabed provides the non-linear geometric restoring force to the floating structure in all degrees of freedom.

Line attachments to the floating structure and the seabed have also been modelled through a set of stiffness ($K_{f/a}$), mass ($M_{f/a}$), damping ($C_{f/a}$) and quasistatic ($F_{f/a}{}^{qs}$) forces which also depend on the structure position, making the relations non-linear. This set of matrices arise from the kinematic constraints imposed on the fairleads and anchors, introduced in the subsequent section in order to show its linearized version.

2.2 System linearization

In order to solve the system (1) in the FD, forces on both the floating structure, the mooring system and line attachments must be linearized. The floating structure and the mooring system are influenced by viscous drag forces which are commonly linearized through harmonic or statistical linearization [9]. Whilst wave interaction forces of the floating structure are modelled through linear potential hydrodynamic coefficients, complemented with a viscous force term, hydrodynamic loads on mooring lines are added through the Morison force, as shown in equation (2). Viscous forces on the floating structure have been included accounting for motions of the buoy, whereas hydrodynamic Morison forces on mooring lines account for the relative motions between water particles and line sections.

On the one hand, the inertial term of the RHS in equation (2) is linear and consists of an excitation force, called effective buoyancy term and proportional to water particles acceleration, and the added mass term, proportional to the acceleration of the corresponding dof of mooring line nodes. On the other hand, the viscous force term in the RHS of equation (2) can be rearranged as an excitation force and a damping force, both functions of the relative velocity of the fluid with respect to the corresponding degree of freedom $\left(u(t) - \dot{\delta}(t)\right)$, as shown in equations (4) and (5). It has been assumed that the current velocity does not significantly contribute on the varying hydrodynamic forces as the floating structure is subject to operational states with a relatively low current. Therefore, assuming that wave particle velocities dominate, the linearized coefficient is introduced in (5) [25]. It makes the viscous drag force non-linear and an iterative procedure is needed to solve the complete FD system.

$$F_{drag}(t) = \gamma\left(u(t) - \dot{\delta}(t)\right) \cdot u(t) - \gamma\left(u(t) - \dot{\delta}(t)\right) \cdot \dot{\delta}(t) \tag{4}$$

$$\gamma\left(u(t) - \dot{\delta}(t)\right) = \begin{cases} \frac{8}{3\pi} \cdot f_v \cdot max\left(u - \dot{\delta}(t)\right) \rightarrow \ Regular\ waves \\ \sqrt{\frac{8}{\pi}} \cdot f_v \cdot \sigma_{u-\dot{\delta}(t)} \rightarrow \ Irregular\ waves \end{cases} \tag{5}$$

In equation (5) $f_v = 0{,}5 \cdot \rho_w \cdot C_d \cdot D \cdot L$ and $\sigma_{u-\dot{\delta}(t)}$ represents the standard deviation of the relative fluid velocity with respect to the corresponding dof. The linearization of the Morison viscous drag term ends up in a set of two linearized forces, proportional to the fluid and to the corresponding dof velocities respectively. The damping matrix and the velocity force depend on all dof motions, implying the FD solution to be solved through a fixed-point iterative process. This iterative method consists in setting an initial value of γ, e.g. 0, that will provide an initial solution and an updated γ. The same computation is carried out until either $max\left(u - \dot{\delta}(t)\right)$ or $\sigma_{u-\dot{\delta}(t)}$, for regular and irregular waves respectively, show a low error with respect to the previous solution, 0.1% has been assumed low enough in this work. Following the same procedure, the inertial forces in equation (2), proportional to the acceleration of the fluid and the corresponding dof, are shown in equation (6). In this case it represents two linear forces that are directly included in the complete FD model, shown in equation (15).

$$F_{mass}(t) = (1 + C_a) \cdot \rho_w \cdot V \cdot \dot{u}(t) - C_a \cdot \rho_w \cdot V \cdot \ddot{\delta}(t) \tag{6}$$

In contrast with the non-linear time domain model, the linearized FD model provides only the time-varying part of the solution. The structural damping, as already introduced in [18], is valid for velocities referred either to the absolute reference centre or to the mean position. However, the stiffness matrix needs to be redefined to work with the time varying motions, referenced to the mean position. Consequently, it implies adapting the structural stiffness matrix of the mooring system as represented in equation (7).

$$[K_G]_n^{n+1} = \begin{bmatrix} [R]_n{}^{n+1} & 0 \\ 0 & -[R]_n{}^{n+1} \end{bmatrix} \begin{bmatrix} [K_L]_n{}^{n+1} & 0 \\ 0 & -[K_L]_n{}^{n+1} \end{bmatrix} \cdot \begin{bmatrix} [R]^t{}_n{}^{n+1} & 0 \\ 0 & -[R]^t{}_n{}^{n+1} \end{bmatrix} \tag{7}$$

$$[K_L]_n{}^{n+1} = \begin{bmatrix} \frac{E \cdot A}{L_0{}_n{}^{n+1}} & 0 & 0 \\ 0 & 0 & 0 \\ 0 & 0 & 0 \end{bmatrix} \tag{8}$$

In equation (7) ‘n’ denotes specific nodes of mooring lines where subscripts and superscripts denote nodes connecting each line section. The subscript ‘L’ indicates local coordinates of each node with the positive ‘x’ direction aligned with a line connecting both nodes, pointing at the node ‘n+1’, as represented in Figure 1. The subscript ‘G’ indicates global coordinates to which the whole system described by equation (1) is referred, with the ‘xy’ plane on the undisturbed SWL and the positive ‘z’ axis pointing upwards as showed in Figure 1. ‘R’ is the rotation matrix relating local and global coordinates for each line section, computed with the floater at the mean position, and K_L is the structural stiffness matrix of each line section referred to its local coordinates. The local structural stiffness matrix accounts only for axial stiffness, and, following the sign convention adopted for local coordinates, it is represented in the first position of the matrix, as shown in equation (8). The structural damping has been defined as a Rayleigh damping matrix. Following the same procedure as in equations (7) and (8) for the stiffness matrix, the structural damping matrix is straightforward defined as $[C_G]_n^{n+1} = \beta \cdot [K_G]_n^{n+1}$, where β is the stiffness proportional Rayleigh damping coefficient.

The non-linear geometric stiffness contributes significantly on the system performance, especially in cases with significant mooring pretensions and in the low frequency (LF) range. Its influence on the floater has been here computed as the secant stiffness force on the floating structure. It is computed after each iteration of the FD, assuming oscillation amplitudes equal to two standard deviations of each degree of freedom of the floater about the mean position, obtaining the floater linearized geometric stiffness matrix, $[K_g^f]$. In addition, the same force differences have also been computed on the mooring line nodes, as a consequence of the same floating structure motion amplitudes, with an analytic subroutine of a catenary mooring system, as described in [26], obtaining $[K_g^m]$. These matrices provide the corresponding geometric stiffness effect on both the floater and lines, as represented in equations (9) and (10).

$$[K_g] = \begin{bmatrix} [K_g^f] & [K_g^m]^T \\ [K_g^m] & [0] \end{bmatrix} \tag{9}$$

$$[K_g^f] = \begin{bmatrix} \frac{\Delta F_1}{\Delta \delta_1} & \cdots & \frac{\Delta F_1}{\Delta \delta_6} \\ \vdots & \ddots & \vdots \\ \frac{\Delta F_6}{\Delta \delta_1} & \cdots & \frac{\Delta F_6}{\Delta \delta_6} \end{bmatrix} \quad and \quad [K_g^m] = \begin{bmatrix} \frac{\Delta F_{dof\_f+1}}{\Delta \delta_1} & \cdots & \frac{\Delta F_{dof\_f+1}}{\Delta \delta_6} \\ \vdots & \ddots & \vdots \\ \frac{\Delta F_{dof\_t}}{\Delta \delta_1} & \cdots & \frac{\Delta F_{dof\_t}}{\Delta \delta_6} \end{bmatrix} \tag{10}$$

In equations (9) and (10) K_g indicates the linearized geometric stiffness matrix based on the mentioned amplitude assumption. The superscripts m and f denote mooring and floater and dof stands for degrees of freedom, assuming that the 'total' degrees of freedom of the coupled system is denoted by dof_t. Summarizing, the stiffness matrix is the static mooring force tensor, considering the influence of motions in all degrees of freedom of the floating structure on all degrees of freedom of the coupled system, both the structure itself and mooring lines.

The kinematic relations, modeling relations between fairlead and anchor points with the floater and the seabed respectively, are defined by means of Lagrange multipliers through the penalty method [21]. It consists in adding a force vector, $\{F_{kin}(t)\}$, that makes the system fulfill the kinematic relations avoiding adding additional equations to be solved.

$$\{F_{kin}(t)\} = \alpha_{kin} \cdot [\Phi_\delta^T(t)] \cdot \left([\Phi_\delta(t)] \cdot \{\ddot{\delta}(t)\} + [\dot{\Phi}_\delta(t)] \cdot \{\dot{\delta}(t)\} + 2\xi_{kin}\omega_{kin}[\Phi_\delta(t)] \cdot \{\dot{\delta}(t)\} + {\omega_{kin}}^2\{\Phi(t)\}\right) \tag{11}$$

In equation (11) the term Φ indicates the kinematic restrictions imposed to the mechanical system, the subscript δ indicates its tensor with respect to each degree of freedom intervening in the restriction, and the dot indicates the time derivative. In the case of mooring lines, these restrictions make the fairleads to keep attached to the corresponding points in the floating structure and the anchors to stay in place at the defined point on the seabed. In the case of diffracting bodies, such as for the floater and the internal SWL, since both have been modelled as six dof rigid bodies, the kinematic relations impose the internal SWL to rigidly move with the floater in surge and sway. Since the internal SWL does not have mass nor stiffness in yaw, it has also been set to rigidly move in yaw with the floater as defined in equation (12) (right) to avoid numerical issues. The numbering of the degrees of freedom of the diffracting bodies has been taken assuming that the 'first' body is the moored body, the floating structure here (dofs 1 to 6), and the second body is the internal SWL (dofs 7 to 12).

$$\{\Phi_{f/a}(t)\} = \begin{Bmatrix} x_{surge} + x_{roll} + x_{yaw} + \delta_{x-fair} - x_n \\ y_{sway} + y_{pitch} + y_{yaw} + \delta_{y-fair} - y_n \\ z_{heave} + z_{roll} + z_{pitch} + \delta_{z-fair} - z_n \\ \delta_{x-anchor} - x_1 \\ \delta_{y-anchor} - y_1 \\ \delta_{z-anchor} - z_1 \end{Bmatrix} \qquad \{\Phi_{dkin}(t)\} = \begin{Bmatrix} \delta_1(t) - \delta_7(t) \\ \delta_2(t) - \delta_8(t) \\ \delta_6(t) - \delta_{12}(t) \end{Bmatrix} \tag{12}$$

Assuming each line of the mooring system is defined by its lumped masses, starting in the anchor (node 1) and ending at the fairlead (node n) (see Figure 1), equation (12) (left) defines all restrictions imposed to it. Each node of a mooring line is defined through its three translational degrees of freedom in the space (x, y, z) and the nodes at the fairleads, nodes '*n'*, must follow the influence of the six degrees of freedom of the (rigid) floating structure on the fairlead position. It is defined through the first three restrictions in equation (12) (left), imposed to the x, y and z positions of the nodes 'n'. In equation (12) $\delta_{x,y,z,-fair}$ denote the position of the

fairlead with respect to the centre of gravity (CoG) of the floating structure as well as $x_{surge,roll,yaw}$, $y_{sway,pitch,yaw}$ and $z_{heave,roll,pitch}$ denote the motions of the fairleads in the global 'x', 'y' and 'z' axis due to the corresponding motions of the floating structure. The anchor points are to be kept fixed on the seabed and to do so the position with respect to the CoG of the floating structure $\delta_{x,y,z-anchor}$ are to be updated along the time.

The simulation in the FD requires all forces to be linear either with respect to the wave amplitude or to the motion of the system. The restrictions in equation (12) can be broken down into two different forces, those depending on system motions and quasistatic force components. Quasistatic forces, specified in (1) through $\mathrm{F}_{\mathrm{f/a}}^{qs}$, are not introduced in the FD model since it is already assumed to be in equilibrium, and consequently $\delta_{\mathrm{x,y,z-fairlead}}$ and $\delta_{\mathrm{x,y,z-anchor}}$ are not considered. Therefore, the restriction vectors (12) can be considered linear at the mean position as $\{\Phi_{f/a}(\mathrm{t})\} = [\Phi_{f/a}] \cdot \{\delta(\mathrm{t})\}$ and $\{\Phi_{dkin}(\mathrm{t})\} = [\Phi_{dkin}] \cdot \{\delta(\mathrm{t})\}$. As long as all restrictions are defined linearly with respect to different combinations of the floater's degrees of freedom the equation (11) becomes equation (13), expressed for the restrictions on mooring line ends $'f/a'$ and on diffracting bodies $'dkin'$.

$$\begin{aligned}\{F_{f/a}(t)\} &= \alpha_{f/a} \cdot [\Phi_{f/a\,\delta}^{T}] \cdot \left([\Phi_{f/a\,\delta}] \cdot \{\ddot{\delta}(t)\} + \left[[\dot{\Phi}_{f/a\,\delta}] + 2 \cdot \xi_{f/a} \cdot \omega_{f/a} \cdot [\Phi_{f/a\,\delta}]\right] \cdot \{\dot{\delta}(t)\} + {\omega_{f/a}}^2 \cdot [\Phi_{f/a}] \cdot \{\delta(t)\}\right) \\ \{F_{dkin}(t)\} &= \alpha_{dkin} \cdot [\Phi_{dkin\,\delta}^{T}] \cdot \left([\Phi_{dkin\,\delta}] \cdot \{\ddot{\delta}(t)\} + \left[[\dot{\Phi}_{dkin\,\delta}] + 2 \cdot \xi_{dkin} \cdot \omega_{dkin} \cdot [\Phi_{dkin\,\delta}]\right] \cdot \{\dot{\delta}(t)\} + {\omega_{dkin}}^2 \cdot [\Phi_{dkin}] \cdot \{\delta(t)\}\right)\end{aligned} \tag{13}$$

The form in which equation (13) is expressed denotes a linear system, which can be included in the FD system (15) straightforward through a set of mass, damping and stiffness matrices ($M_{f/a}$; $C_{f/a}$; $K_{f/a}$; M_{dkin}; C_{dkin}; K_{dkin}). It should be noted that this formulation can also be used to set restrictions between several floating structures, as it has been done here for the diffracting bodies (the structure and the internal SWL), through additional restrictions to those set in equation (12) (right). Unlike the mooring system, restrictions imposed on the diffracting bodies are proportional to the body motions and no constant forces have been needed in the TD model.

The slowly varying second order wave drift forces have been included in the linearized model through the spectrum proposed in [27]. It has also been introduced here in equation (14), where S_{η} and S_{SV} denote the spectra of the wave elevation and of the slowly varying wave drift force respectively.

$$S_{SV}(\mu) = 8 \cdot \int_0^{\infty} S_{\eta}(\omega + \mu) \cdot S_{\eta}(\omega) \cdot |T(\omega + \mu, \omega)|^2 \cdot d\omega \tag{14}$$

The Froude-Krylov and diffraction force (F_w) and the radiation force (F_{rad}) have been computed as linear forces in the TD model introduced in section 2.1. Consequently, the same forces, expressed in the FD have been used in equation (15). The former is computed with the wave force per unit amplitude, obtained with the potential flow commercial software [17] as $F_w = \hat{F}_{w-R.A.O.}(\omega) \cdot \hat{\eta}(\omega)$ and, for the latter, the radiation force coefficients in the FD are used, as detailed in equation (15), through the added-mass $A(\omega)$ and radiation

damping $B(\omega)$ coefficients, with the clear advantage of avoiding the computation of the convolution force, required by the radiation force in the TD.

The seabed vertical reaction force is modelled in the FD through stiffness and damping matrices on the nodes in contact with the seabed, with values providing a natural frequency of the vertical motion equal to 10[rad/s] and critically damped. The horizontal friction force has been modelled through a damping matrix acting on the horizontal degrees of freedom of the corresponding nodes of each mooring line, with the same damping coefficient obtained for the vertical reaction, assuming the same properties of the seabed in all directions. These matrices have been included in the mooring stiffness and mass matrices.

The resulting coupled mechanical system can be expressed as in (15), where it has been added a subscript to the linearized damping γ values to distinguish viscous damping on floating structure and on mooring nodes.

$$\begin{aligned}\left(-\omega^2\cdot\begin{bmatrix}\left(M+A(\omega)\right)_{str}+M_{dkin} & M_{f/a}\\ M_{f/a} & M_{moor}+\rho_w\cdot V\end{bmatrix}+i\omega\cdot\begin{bmatrix}\gamma_{str}\left(u(t)-\dot{\delta}(t)\right)+B(\omega)+C_{pto}+C_{dkin} & C_{f/a}\\ C_{f/a} & C_{moor}+\gamma_{moor}\left(u(t)-\dot{\delta}(t)\right)\end{bmatrix}\right.\\ \left.+\begin{bmatrix}H_{str}+K_g^f(\delta)+K_{pto}+K_{dkin} & K_g^{mT}(\delta)+K_{f/a}\\ K_g^m(\delta)+K_{f/a} & K_{moor}\end{bmatrix}\right)\cdot\begin{Bmatrix}\hat{\delta}_{str}(\omega)\\ \hat{\delta}_{moor}(\omega)\end{Bmatrix}\\ =\begin{Bmatrix}\hat{F}_{w-R.A.O.}(\omega)\cdot\hat{\eta}(\omega)+\hat{F}_{sv}(\omega)\\ \left(-\omega^2(1+C_a)\cdot\rho_w\cdot V+i\omega\cdot\gamma_{moor}\left(u(t)-\dot{\delta}(t)\right)\right)\cdot\hat{\eta}(\omega)\end{Bmatrix}\end{aligned} \tag{15}$$

Since equation (15) contains both damping and stiffness terms dependent on the solution, the whole system is solved iteratively, through the fixed point iteration procedure as detailed above in this section. Therefore, the resulting solution yields constant values of the mentioned solution dependent terms.

3 Floating Wave Energy Converter numerical model

The model described above has been applied to a floating WEC which consists of a two-body floating spar type OWC, assumed to be a rigid structure. It is a cylindrical structure with an internal water column which communicates the sea water with an air chamber at the top. Waves' motions excite the floating structure in heave as well as its internal water column, the air in the air chamber at the top of the water column is compressed and forced to be passed through an air turbine. The energy yielded in the air turbine, is transformed into electrical power that can be exported onshore.

3.1 Linear Potential Model

The hydrodynamic coefficients of the floating WEC have been obtained with the commercial BIEM code [17], as it is carried out in the equivalent non-linear TD model. Two diffracting bodies have been modelled, the first body (dofs 1 to 6) represents the geometry of the spar, shown in Figure 2. The outer diameter specified in Figure 2 refers to the larger diameter of the floater both at the top and at the bottom, the OWC diameter indicates the diameter of the internal water column, all dimensions are defined in [15], model 'K' and also used as a case study in [5]. The second body in the numerical model (dofs 7 to 12) is a massless surface at the internal water surface to model its motions.

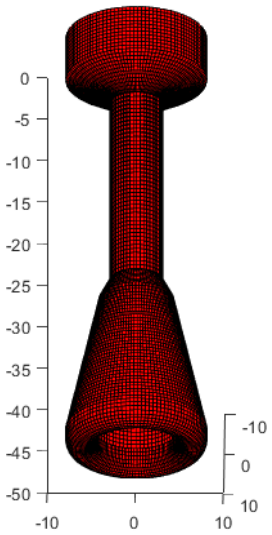

Structure Main Properties	
Total mass [kg]	$2.4432 \cdot 10^6$
CoG [m]	*-31.97*
Draft [m]	*40.81*
Mass Moment of Inertia [kg·m2]	$190.93 \cdot 10^6$
Outer Diameter [m]	*16*
OWC diameter [m]	*5.89*

Figure 2. Floating Spar type oscillating water column. Geometry specified in [15], model 'K' (left) and main physical properties of the floating structure (right)

In order to model the internal water surface horizontal motions, in surge, sway and yaw, rigidly with the spar structure, three kinematic restrictions have been imposed to both bodies as described by equation (12) (right). Additionally, they have been left to move independently in heave, roll and pitch. The PTO has been assumed to be linear and acting on the relative heave motions between the floating structure and the internal SWL in both the TD and the FD models. The PTO represents a real system that any WEC needs in order to transform the mechanical power in the buoy motion into electrical power to be delivered into the grid. Such power transformation needs to be performed through an opposing force that will significantly influence WEC's motions. In principle, the PTO force needs to be purely resistive so that there is no power backflow from the PTO to the buoy. However, some PTO systems may introduce an additional stiffness term that makes it to introduce power into WEC's motions during short periods of time. In order to model these two properties it is usually introduced a set of stiffness and damping matrices (K_{pto}, C_{pto}), as represented, in the time and FDs, in equation (16).

$$F_{pto}(t) = K_{pto} \cdot \left(\delta_3(t) - \delta_9(t)\right) + C_{pto} \cdot \left(\dot{\delta}_3(t) - \dot{\delta}_9(t)\right) \;\rightarrow\; F_{pto}(\omega) = \left(K_{pto} + i\omega \cdot C_{pto}\right) \cdot \left(\hat{\delta}_3^{f}(\omega) - \hat{\delta}_3^{SWL}(\omega)\right) \tag{16}$$

The PTO in an OWC system consists generally of a self-rectifying air turbine, such as the Wells turbine or Impulse turbines as introduced in [28], [29], that just introduces a damping term in the relative motion. In addition, the air chamber compressibility adds a non-linear stiffness term in the relative motion. In this work it has been considered just a damping term for simplicity, assuming the chamber not to introduce any stiffness in the system, which can be acceptable for the mooring induced loads but has a non-negligible influence in the produced power [30]. The optimal PTO damping to maximise the extracted energy has been computed with the FD model, accounting only for the body motions in heave, with the corresponding linearized drag coefficients, and without the mooring system. The PTO damping has been found through a numerical

maximisation of the power in each of the simulated sea states showed in Figure 7, the obtained values are represented in Figure 3.

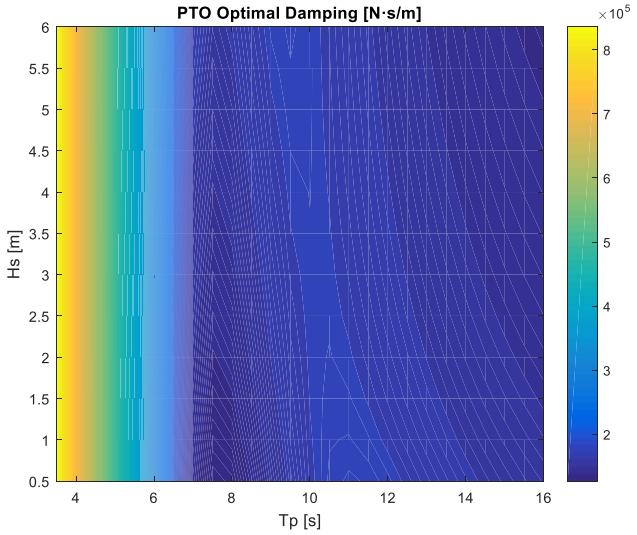

Figure 3. Optimal PTO damping per sea state computed with the OWC type WEC represented in Figure 2

The total mass of the floating structure is $2.4432 \cdot 10^6$[kg] and the Centre of Gravity (CoG) is placed 31.97[m] below the surface water level, assuming to be similar to the geometry introduced in [16]. The mass moment of inertia in pitch and roll has been assumed to be $190.93 \cdot 10^6$[kg·m^2] derived from assuming a radius of gyration equal to half the length of the section from the CoG to the keel, 8.84[m].

The motions of the floating structure are influenced by viscous drag forces as specified in equation (4), the corresponding factors are described in Table 1 along with the natural frequencies in each degree of freedom, computed through the modal analysis introduced in section 4.1, considering the mooring system. Viscous drag force factors have been computed as indicated for equation (5), assuming a drag coefficient of each circular section of the WEC in all directions of $C_d = 0.8$. It implies a wake amplification factor with respect to the steady current drag coefficient selected in section 3.3 equal to 1.23, within the recommendations in [31].

Table 1 Viscous drag force factors considered for each degree of freedom of the floating structure

Degree of freedom	***Viscous Drag Factors f_v [N·s/m] // [N·m·s]***	***Natural frequencies [rad/s]***
Surge	*$1.188 \cdot 10^5$*	*0.064*
Sway	*$1.188 \cdot 10^5$*	*0.065*
Heave	*$4.469 \cdot 10^4$*	*0.6651*
Roll	*$3.532 \cdot 10^9$*	*0.3757*
Pitch	*$3.532 \cdot 10^9$*	*0.3757*
Yaw	*0*	-
Heave SWL	*0*	*0.5063*

Roll SWL	*0*	*2.524*
Pitch SWL	*0*	*2.524*

3.2 Catenary Mooring System

The mooring system for the model verification has been assumed to be made up of three catenary lines as specified in Table 2 and represented in Figure 4, in a water depth of 172m, 140m below the fairleads. The corresponding lines are made up of a single chain section with the properties specified in Table 3 and also assumed in the tank test validation introduced in [18]. The corresponding non-dimensional pretension of the lines is 1.43[-] as defined in [26].

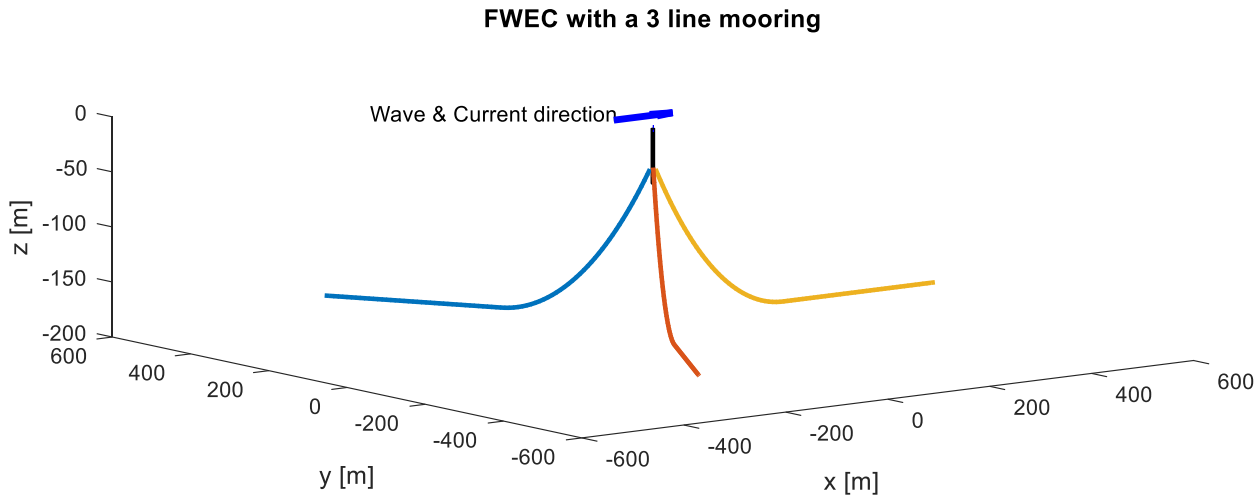

Figure 4. Floating WEC with the three-line mooring system. The wave and current propagation direction are represented with a blue arrow along the positive 'x' axis.

Table 2 Mooring line lengths, fairleads and anchor points

Property	***Line 1***	***Line 2***	***Line 3***
x_fairlead [m]	*-1.5*	*-1.5*	*2.9*
y_fairlead [m]	*-2.6*	*2.6*	*0.0*
z_fairlead [m]	*-32.0*	*-32.0*	*-32.0*
x_anchor [m]	*-277.0*	*-277.0*	*554.0*
y_anchor [m]	*-479.8*	*479.8*	*0.0*
z_anchor [m]	*-172.0*	*-172.0*	*-172.0*
Length [m]	*590.0*	*590.0*	*590.0*

Table 3 Mooring line properties

Property	***Value***
Equiv. Young Modulus [Pa]	$3.35 \cdot 10^{10}$
Equiv. A [m2]	$1.78 \cdot 10^{-2}$
Linear mass density [kg/m]	*140*
Rayleigh Damp Coeff [-]	*0.001*

Seabed friction coeff [-]	*0.5*
Ca [-] (axial)	*0.5*
Ca [-] (radial)	*1*
Cd [-] (axial)	*0.6389*
Cd [-] (radial)	*1.33*
Hydrodynamic Diameter [m]	*0.151*

In order to select the appropriate number of line sections and the integration time step, a sensitivity study has been carried out. The resulting time series with increasing number of sections are showed in Figure 5 for fairlead tensions of lines 1 and 3 and surge. The relative error of the corresponding standard deviations with increasing number of line elements are plotted in Figure 6. Lines discretization with 15 elements show relative errors below 5% both in lines tension and in surge motion. Therefore, it was decided to consider mooring lines made up of 15 sections, as a trade-off between computational time and accuracy, totalling a second order coupled system of ordinary differential equations of 156 degrees of freedom (48 per line and 6 per diffracting body).

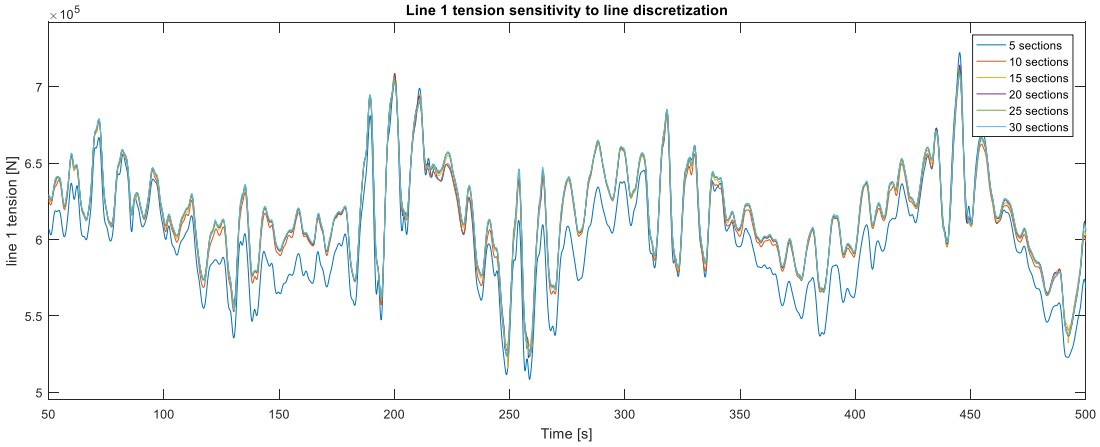

a)

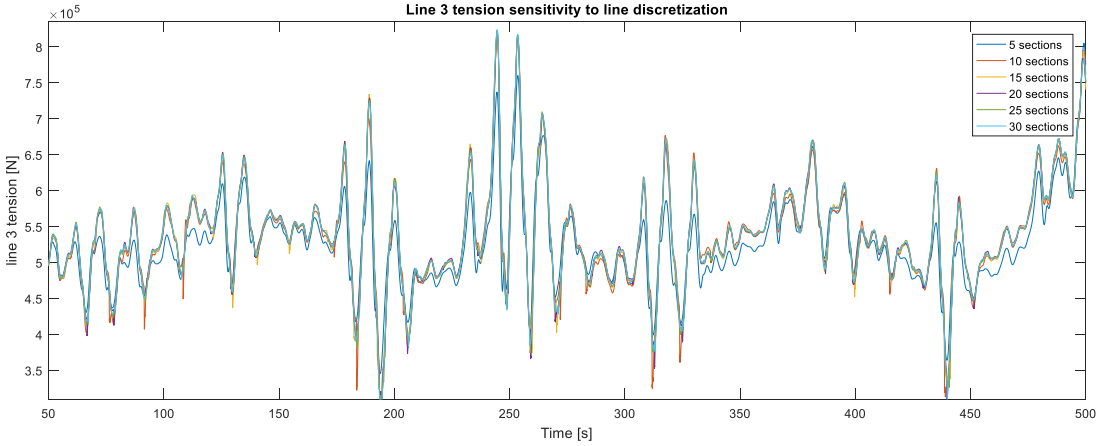

b)

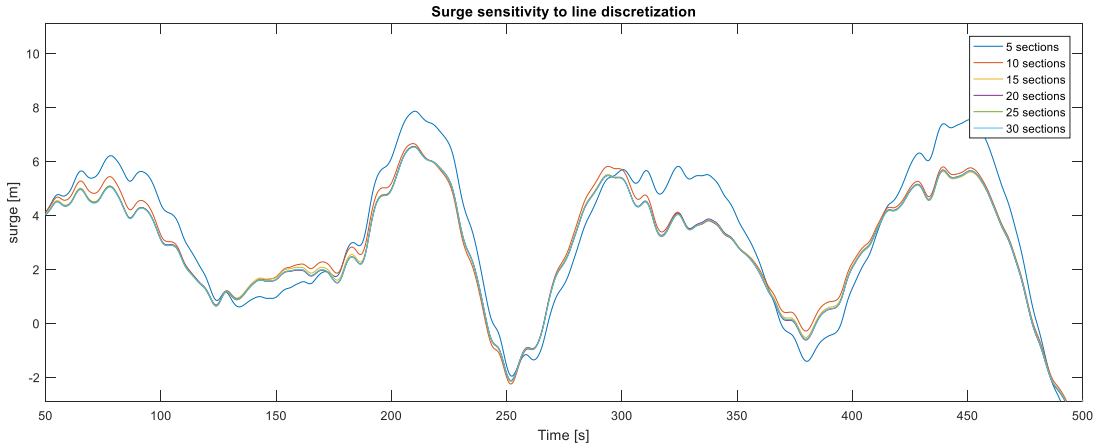

c)

Figure 5. Resulting time series of the sensitivity analysis to the number of sections used to discretize each mooring line. Time series of line 1 a), line 3 b) and surge c)

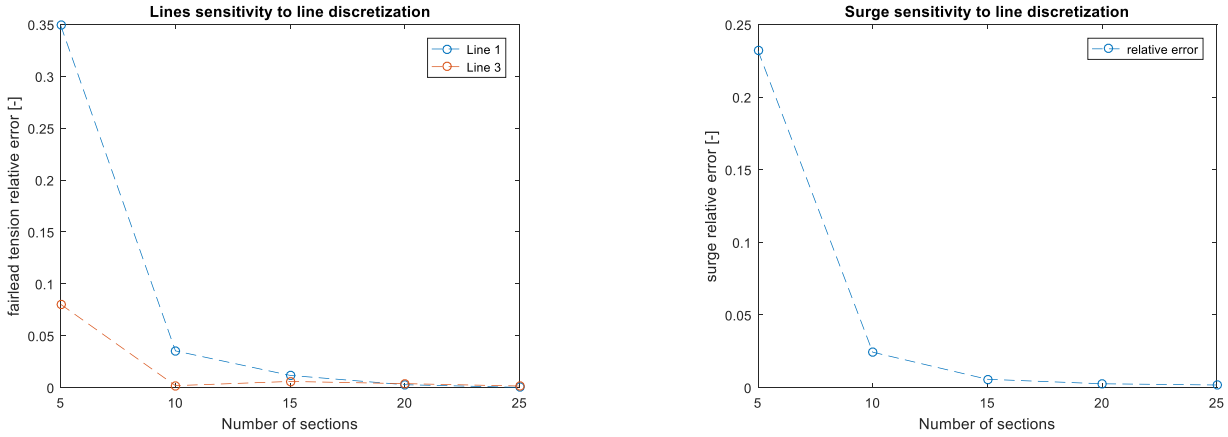

a) b)

Figure 6. Relative errors found in standard deviations of the sensitivity analysis to the number of line sections. Relative errors of the standard deviations of lines 1 and 3 a) and surge b)

In addition, a simulation with 15 sections and half the time step, 0.01s, has been performed. The relative error of the standard deviation of the simulation with the original time step with respect to the simulation with a time step of 0.01s has been checked for the surge motion and tensions of lines 1 and 3. The error in surge was found to be of $7.3 \cdot 10^{-3}$% while in line tensions of lines 1 and 3 were $7.6 \cdot 10^{-2}$% and $3.7 \cdot 10^{-2}$% respectively. Therefore, it has been decided to maintain the time step in 0.02s for all the verification cases. Even though stiffness and damping of the seabed interaction model also influence line tensions, it has been verified in [18] that the results are acceptably accurate with the assumed values, specified in section 2.2.

3.3 Environmental conditions

The WEC here analyzed has been subject to the most occurrent (>1% annual time) sea states at the BiMEP test site [19], which are pointed out Figure 7. It covers 63% of the annual time with a reduced number of simulation cases, 36 sea states, which also cover a wide range of Hs and Tp values, considered enough for verification in operational conditions. In the performed simulations the current and wave propagation

directions have been assumed aligned with the global ‘x’ axis, in the positive direction, as specified in Figure 4.

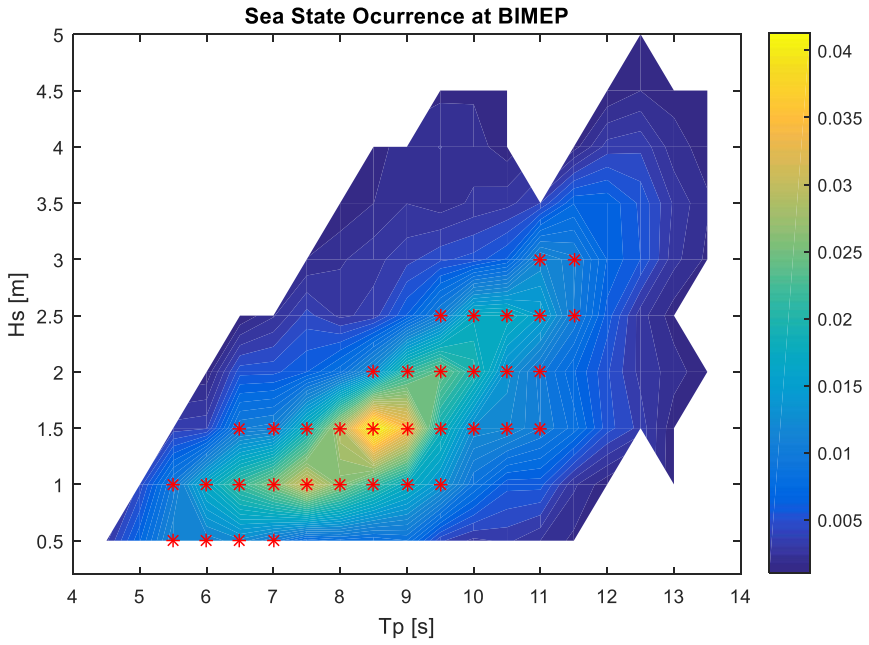

Figure 7. Sea State Occurrence probability at BIMEP test site [19] and a total of 36 Sea States with more than 1% occurrence probability (red stars), selected for TD and FD simulation comparison

The spectral shape considered has been a JONSWAP with a gamma factor of 3.3 in all sea states. The current force has been considered as a steady force, modelled as in the third term of the RHS in equation (2), induced by the mean current speed, assumed constant with the draft of the WEC as it is relatively lower than the water depth. A representative current speed in operational conditions of 0.5m/s has been assumed. The frontal area of the submerged part of the WEC in the current direction is 290[m^2] and a common drag coefficient for smooth cylinders of 0.65 has been assumed.

4 Results

The results of simulations in the FD with the model introduced in (15) have been compared with the corresponding simulation in the TD of the non-linear coupled model described by equation (1). Results in terms of motions and line tension power spectral densities (PSDs) are compared and differences have been quantified through the relative error of standard deviations of the FD model with respect to the non-linear TD model. WEC and mooring performance have been obtained with 12 one-hour TD simulations, assumed to be large enough to represent some hundreds of LF cycles to provide good PSDs. An additional initialization period of 500s has been simulated in each realization that has been disregarded for the PSD computations. The PSDs of the time series have been computed through the *‘pwelch’* subroutine within the Matlab software [32], using the 12 simulations. Since the FD model has been linearized, an eigenvalue and eigenvector analysis has been carried out and is subsequently presented. It allows a deeper analysis and understanding of the extent of the applicability of the linearized model.

4.1 Modal Analysis

Even though the natural frequencies related with surge and sway change with the mean position of the floating structure, a relevant sea state has been selected to analyse the modes of motion of the coupled system, Hs=1.5m and Tp=8.5s, which corresponds with the most occurrent sea state at the selected site.

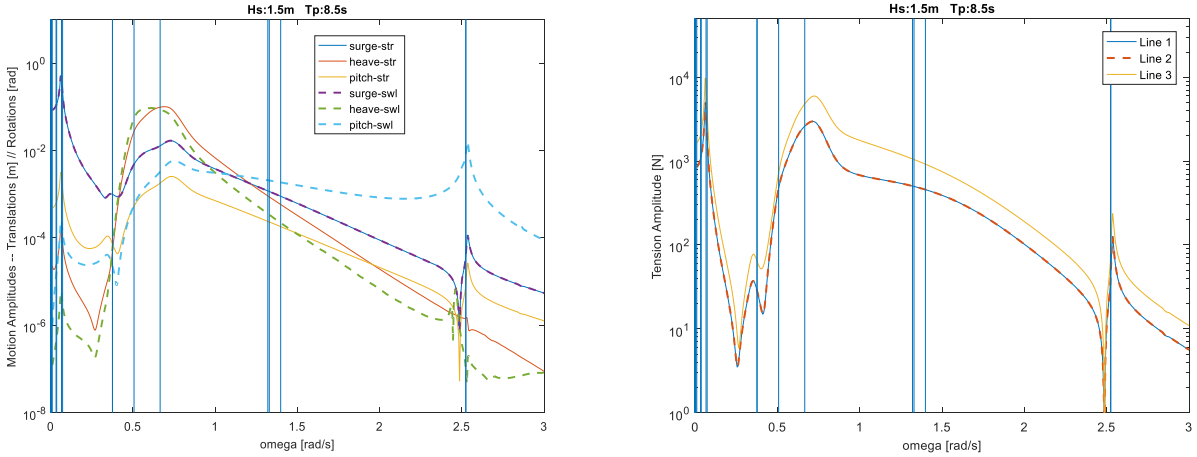

Figure 8. Floating structure and internal surface water level motion amplitudes (left), lines tension amplitudes at the fairleads (right) and eigenvalues within the showed frequency range (vertical lines). Response amplitudes subject to a sea state of Hs=1.5m and Tp=8.5s

Figure 8 has been here introduced in order to visualize the relation between the dofs of the WEC and the induced line tension amplitudes, subject to a representative sea state. Since the wave propagation direction does not excite sway, roll and yaw motions, these have been omitted in the figure. The most relevant eigenvalues have been considered to be those influencing most the motions and tension amplitudes, all showed in Figure 8, with the vertical axis in logarithmic scale in order to visualize the correlation between motions, line tensions and eigenvalues.

It is clearly appreciated that the first peak in all motion and tension responses has two related eigenvalues. More precisely, the two modes of motion around this frequency, 0.065rad/s as represented in Figure 9.

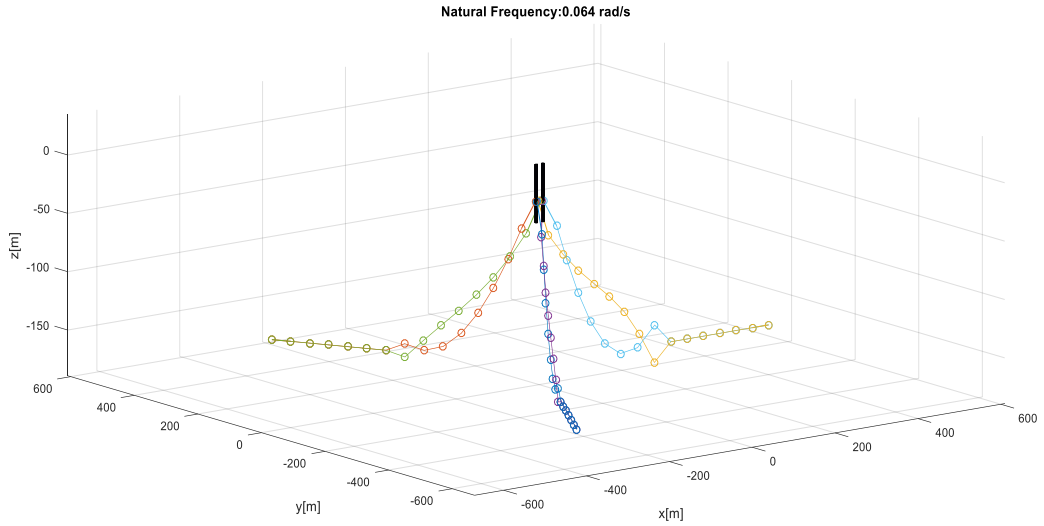

Figure 9. Modes of the coupled system mainly related with surge (top) and sway (bottom)

The modes represented in Figure 9 are mainly related with surge and sway motions of the WEC. However, with the wave direction aligned in the positive 'x' axis, the mode related with the surge motion is mostly excited and, therefore, the one producing the tension peak around the corresponding frequency. It should be noted that, even though the mean position of the floating structure subject to specific environmental conditions provides different stiffness in surge and sway, both natural frequencies have been found very close to each other. Nevertheless, whilst the mode related with surge excites the three lines, the one related with sway excites only the two front lines. This statement should also be verified with small bending stiffness in the mooring lines. These modes of motion induce significant motions of lines' nodes which may be overdamped due to drag force linearization in the FD model when subject to specific sea states.

A group of other 4 frequencies are found around 0.5rad/s shown in Figure 8, related with heave of the floating structure, heave of the internal SWL, pitch and roll motions, as represented in Figure 10 and Figure 11 respectively. It should be noted that the heave of the internal surface water level corresponds with the piston

mode in absolute coordinates, and the power is generated from the relative heave motion between the structure and the internal SWL.

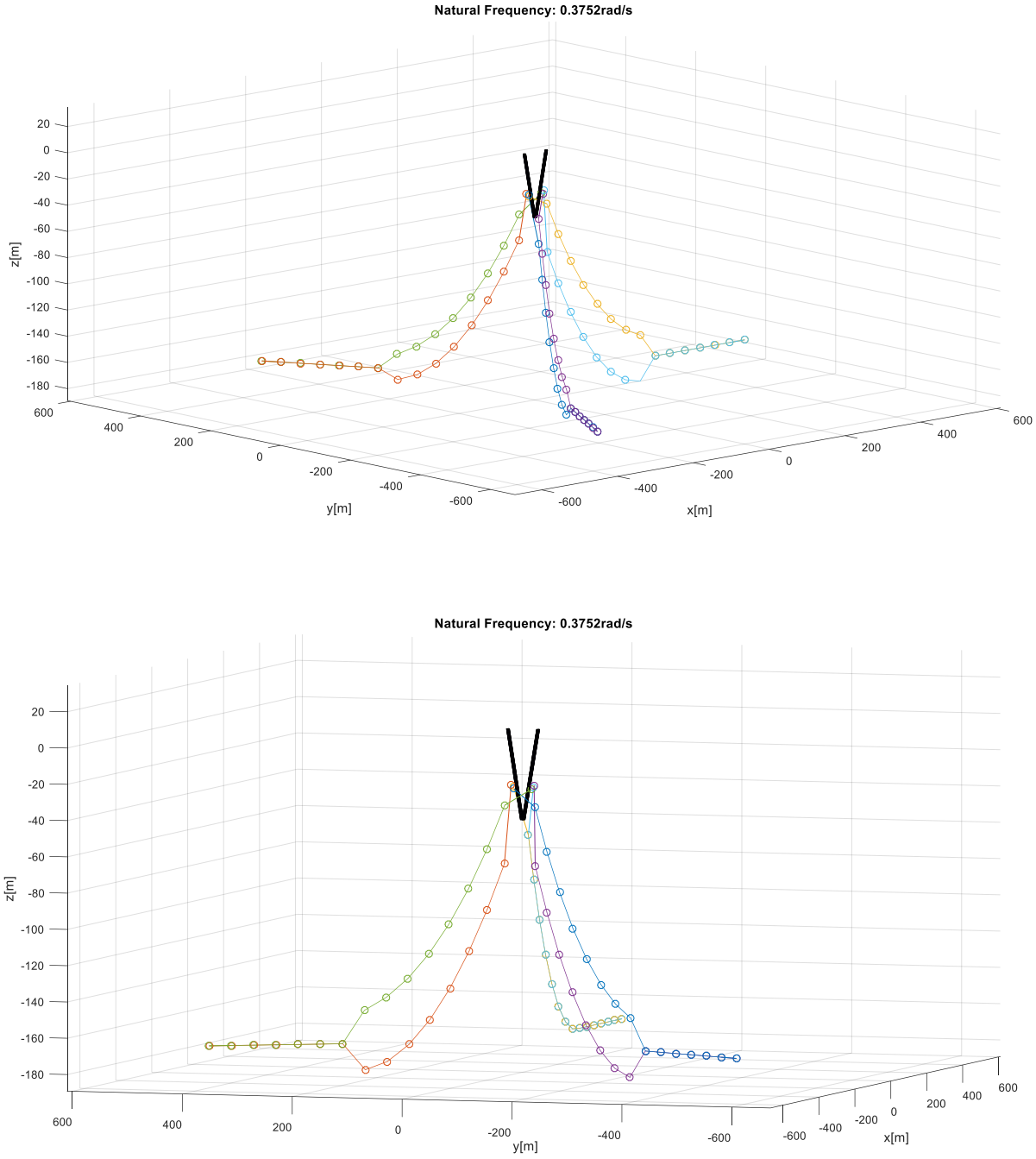

Figure 10. Modes of the coupled system mainly associated with pitch (top) and roll (bottom)

Modes related with pitch and roll motions, as stated for surge and sway, induce significant line motions. These modes can induce differences in the mooring induced damping due to the linearization of drag forces on lines. However, it is not clearly shown in FD computed motion responses nor in line tensions, very likely as a consequence of being overdamped by the linearized viscous damping of the floating structure.

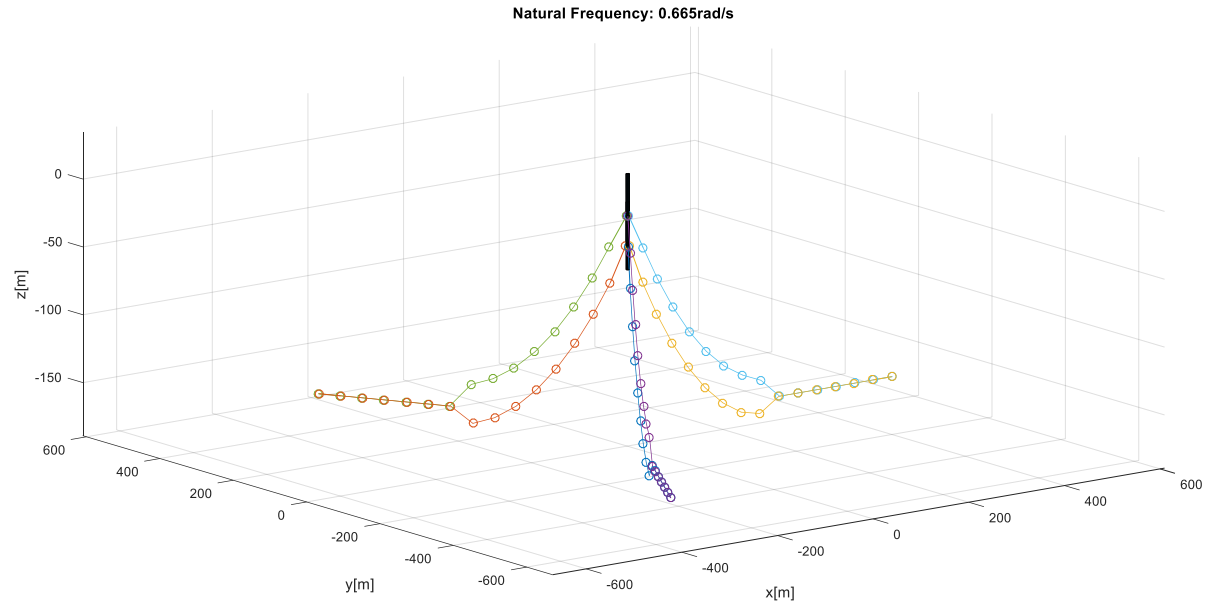

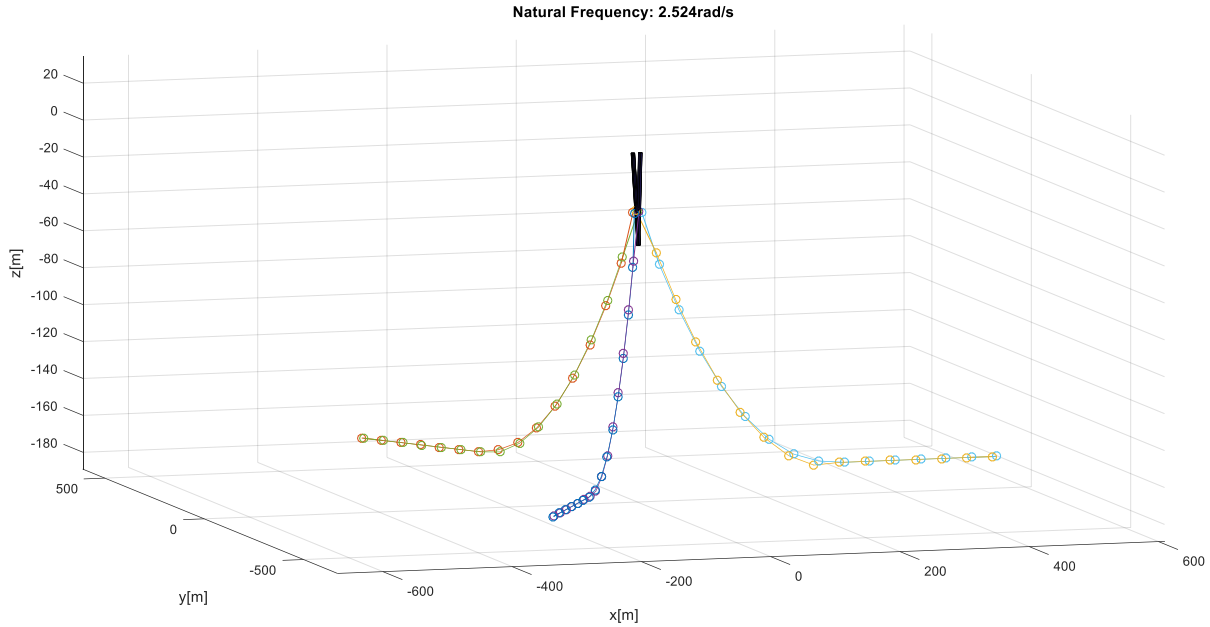

Figure 11. Modes of the coupled system mainly associated with heave of the floating structure (top) and pitch of the surface water level (bottom)

The modes related with floating structure and SWL heaving motions are represented in Figure 11 (top) which, unlike surge and sway, do not excite significantly lines motions. On the other hand, the floating structure is significantly excited by waves and, consequently, large tension amplitudes can be observed in line tensions in Figure 8 (right). The modes related with the internal SWL pitching, influence line tensions as they are coupled with the floating structure pitch and surge. It is clearly shown that all modes experience some excitation at such frequency in Figure 8. However, this frequency should be related with the corresponding sloshing mode in a more realistic numerical model. It has been found at a relatively large frequency and its influence on line tensions can be assumed not to be relevant.

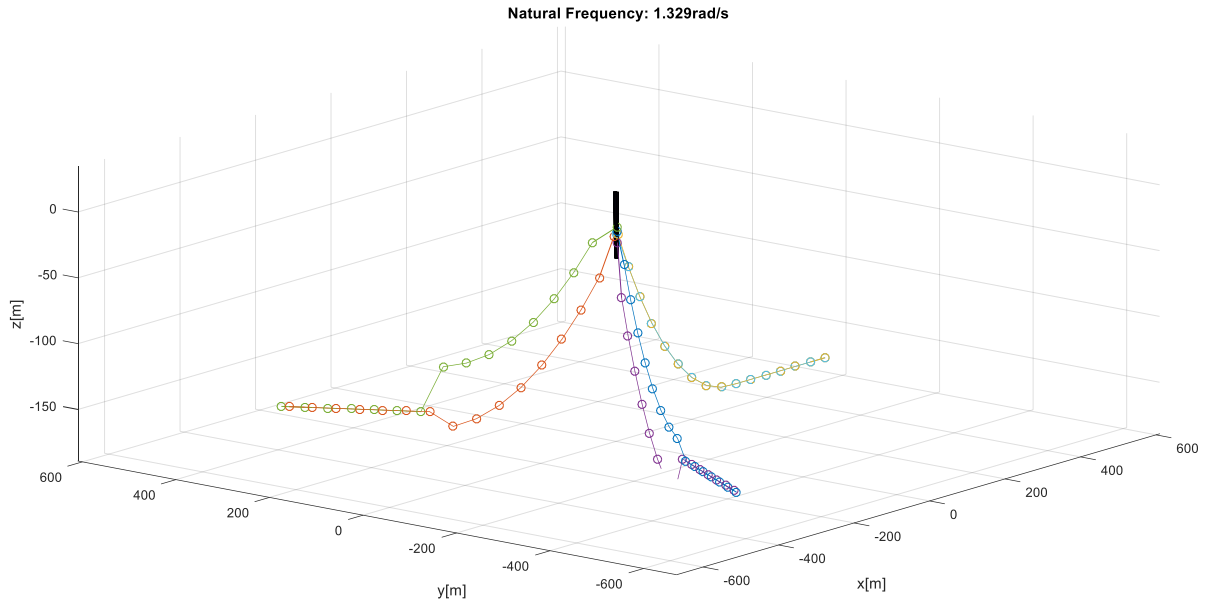

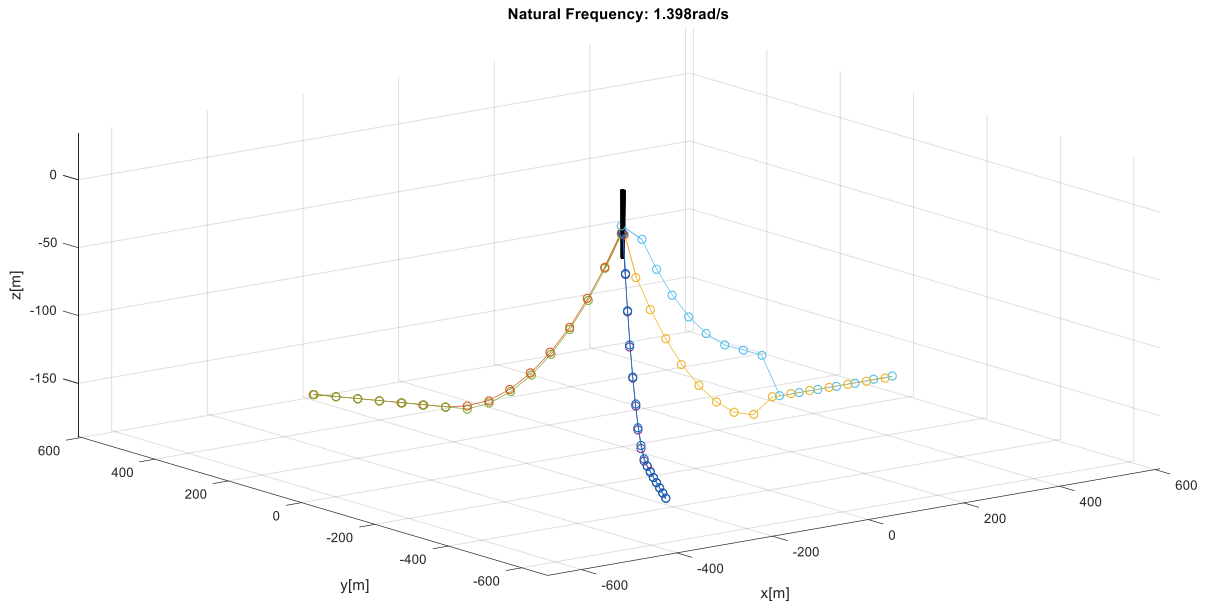

Figure 12. Modes of the coupled system associated with line motions in the plane of the catenary of the windward lines (top) and the leeward line (bottom)

The modes represented in Figure 12 are related with in-plane lines motions with no significant motion of the floating structure. Both modes have been found to be in similar frequencies as the mean position of the floating structure has been relatively small, of 0.8372m, and the shape of the three lines is similar at that position. A third mode has been found at 1.32rad/s, omitted here, which shows a combination of both modes showed in Figure 12 in opposing phase. These three modes are related with some differences between FD and TD models here compared, as can be observed in line tension PSDs in Figure 19 in the corresponding frequency range. The modes of motion showed in Figure 12 correspond with an axial mode, stretching the whole line. Although with the FD model lines tension PSDs show a smooth decrease as the frequency is increased over these natural frequencies, the TD model show a steep decrease in the same range, especially in low energy sea states. This

discrepancy can be attributed to non-linearities not appropriately caught in the linearized FD model, such as the interaction with the seabed or lifting line sections from the seabed. Moreover, it can cause overestimations in line tension standard deviation values of around 20% with low incoming energy, as shown in Figure 19. On the other hand, the explained discrepancy is balanced by the increasing line tension induced by the heaving motions as the Hs is increased. Therefore, it is relevant under low Hs sea states.

4.2 Floater Motions

Surge, heave and pitch motions of both the floater and the internal SWL have been compared between both models in terms of their PSDs and the percentage difference of their standard deviations.

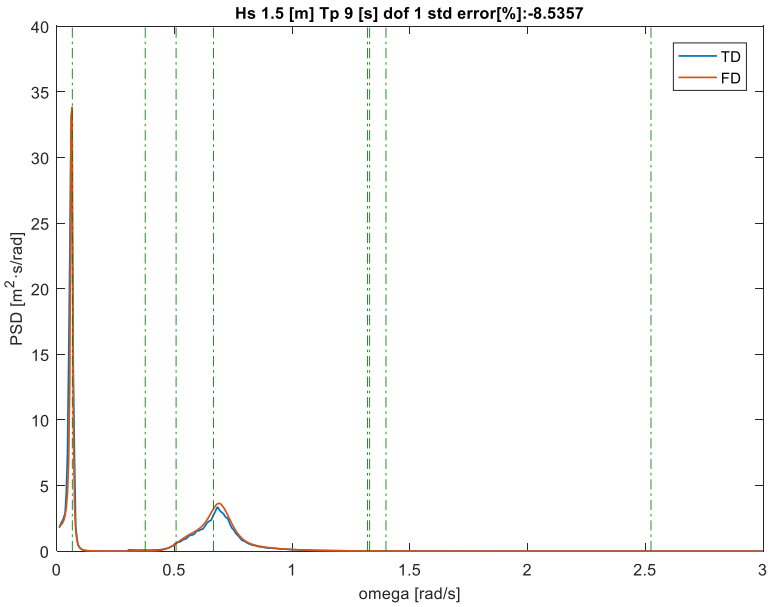

Figure 13. Surge motion PSDs of the floater. Wave frequency magnified with a factor of 100 to enable plotting the whole PSD in a single figure. Dash-dotted vertical lines indicate the relevant modes identified in section 4.1

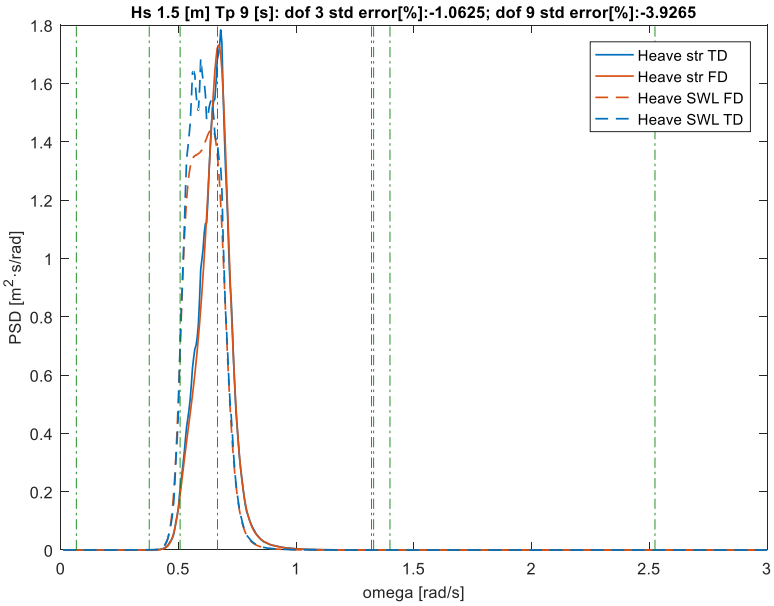

Figure 14. Heave motion PSDs of the floater (solid lines) and the internal SWL (dashed lines). Dash-dotted vertical lines indicate the relevant modes identified in section 4.1

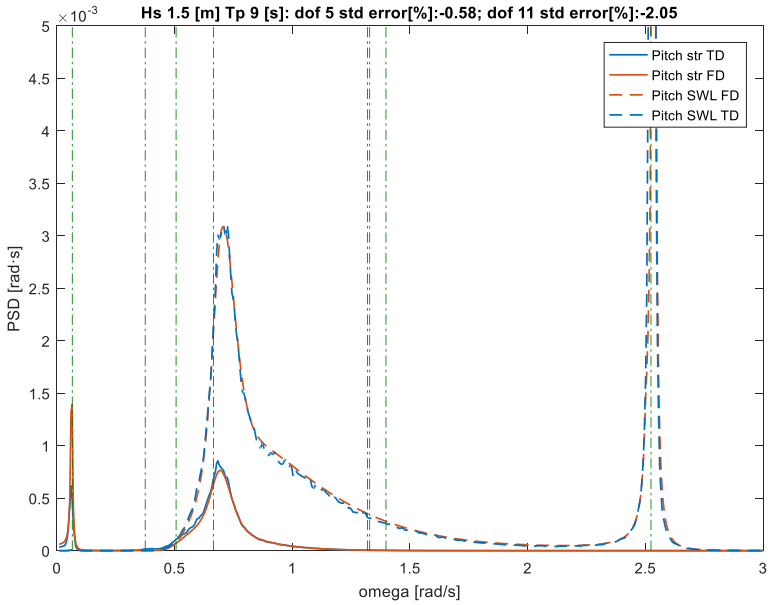

Figure 15. Pitch motion PSDs of the floater (solid lines) and the internal SWL (dashed lines). Dash-dotted vertical lines indicate the relevant modes identified in section 4.1

Looking at the natural frequencies related with each degree of freedom of the floating structure and the internal SWL in Table 1, the peaks of the motions can be associated to each natural frequency. The peaks of the response in surge and pitch at frequencies of 0.065[rad/s] correspond with the natural frequency in surge, which indicates that both modes are coupled. As the peak period of the sea state showed in Figure 13 to Figure 15 is 9 seconds both heaving natural frequencies are significantly excited, this is shown in Figure 14 as the internal SWL is most amplified in frequencies close to 0.5[rad/s] and the floating structure heaving at frequencies close to 0.66[rad/s]. The pitching motion of the floating structure is not clearly shown in Figure 15 as there is no significant excitation around this frequency. In contrast, the pitching motion of the internal SWL, which corresponds to a sloshing mode, is clearly shown around its natural frequency of 2.524[rad/s], mostly due to not having introduced any viscous force in it.

The natural frequency in surge show good agreement between both models in Figure 13. It indicates that the linearized stiffness matrix introduced by the analytic mooring system represents well the mooring influence on the floating structure. The kinematic relations are well fulfilled as both models show negligible differences in surge, what can be observed in Figure 8, and consequently the surge of the water column has been omitted in Figure 13. However, the uncertainties in surge can be mostly attributed to the magnitude of motion in its natural frequency, consequence of differences on the mooring induced damping.

It is shown in Figure 15 that the pitching of the floater in the linearized model is overestimated in the LF range, balanced by the underestimation in the wave frequency (WF) range. While the former is due to overestimates in surge, the latter can be attributed to the linearization of the viscous force term, which tends to overdamp the response. In addition, it is shown in Figure 16 that the pitch motion of the floater is underestimated when subject to more energetic sea states, amplifying the differences in pitch within the WF range.

Pitch of the internal SWL shows very good agreement as it is not directly influenced by the most relevant non-linearities, however, it corresponds with a sloshing mode of the surface and it may be largely influenced by the air chamber pressure, which has not been considered here.

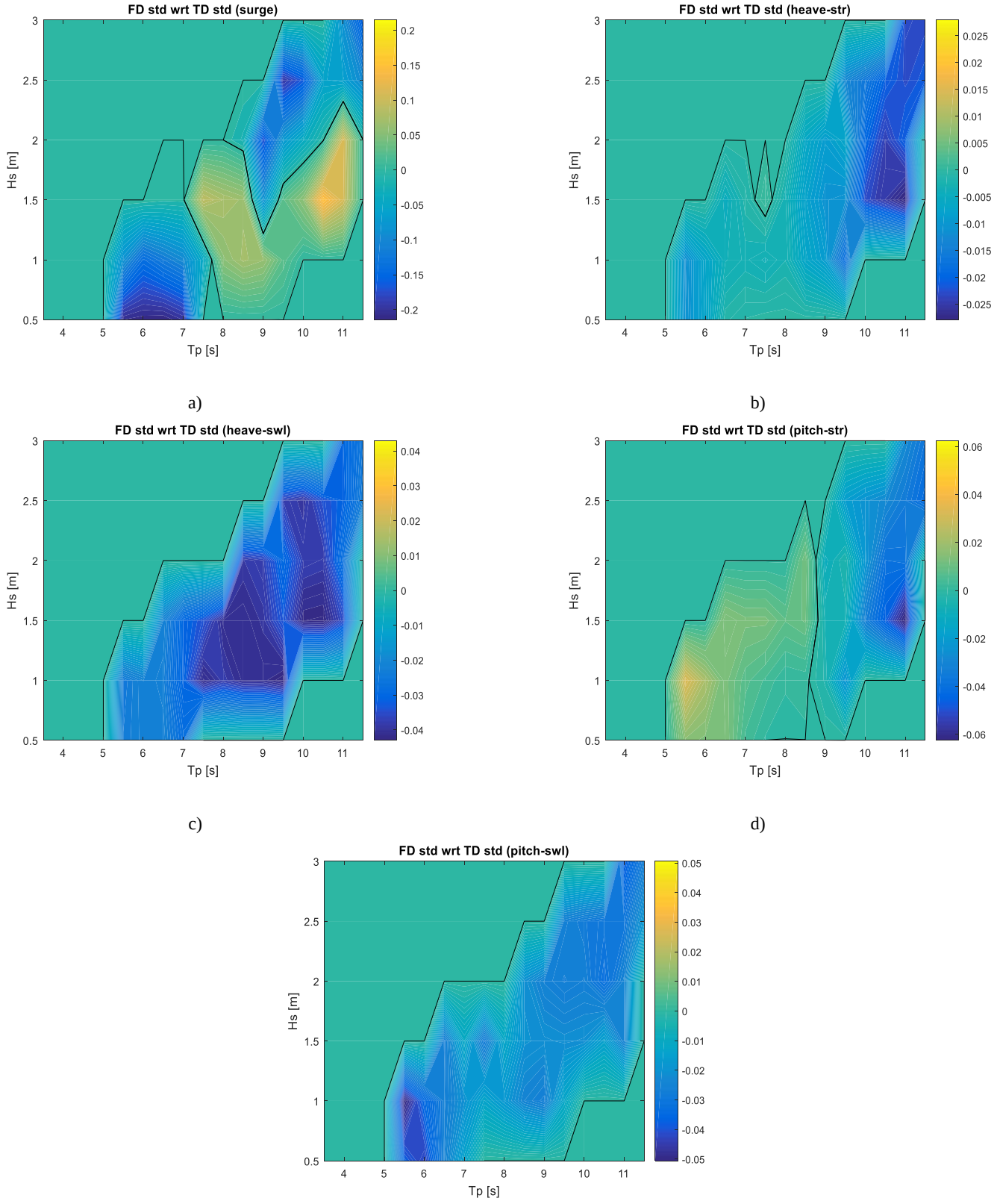

a) b) c) d) e)

Figure 16. Percentage differences of the standard deviation of motions of the linearized FD model with respect to (wrt) the non-linear TD model. Contour lines represent zero levels, showing both limits of the selected simulation sea states and limits between under and overestimations of the FD model. a) Surge; b) Heave of the floating structure; c) Heave of the internal surface water level; d) Pitch of the floating structure; e) Pitch of the internal surface water level

All degrees of freedom show in Figure 16 differences lower than 6% in standard deviation with respect to the non-linear TD model except surge. Surge, unlike other degrees of freedom, is very influenced by non-linear effects such as slowly varying wave drift forces and the geometric stiffness, what explains its larger differences. Additionally, the modes of motion related to surge and sway imply significant lines motions, as showed through modal analysis in Figure 9, and the inherent error made in the linearization of viscous forces on lines may vary the induced damping on floating structure motions. Mentioned effects makes surge to be overestimated in most sea states, as a consequence of overestimations in the LF range and its high relevance on the standard deviation with respect to WF motions.

Heave motions although slightly underestimated in intermediate wave heights are in general in very good agreement, both of the floating structure and the SWL. Observed differences can be mostly attributed to being overdamped by the linearized viscous drag.

4.3 Line Tension

Line tension PSDs can be derived from nodes' motions both in the LF and in the WF range. The geometric stiffness linearization allows catching the induced line tensions in the LF range. As stated for pitch motions, line tensions are overestimated by the FD models in sea states with lower energy content. Similarly, the deviations in the WF range drives the total standard deviation percentage difference as the incoming wave energy increases, as represented in Figure 18 and Figure 19.

Heaving motions are significantly excited, and a more non-linear behaviour of lines can be expected. Line tension amplitudes obtained in frequencies (0.5-0.7rad/s) corresponding to heave natural frequencies are acceptably well represented by the linearized model in Figure 19, specially for the windward lines, while the leeward 'line 3' shows larger differences, more influenced by WF motions.

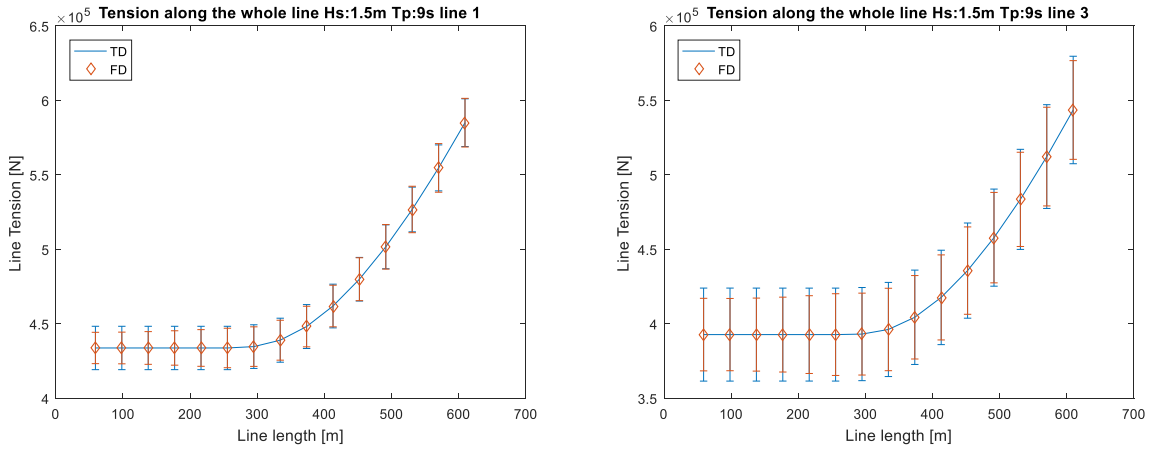

Figure 17. Line tension standard deviation (vertical lines at each node) with both models with respect to the mean line tension along the whole line 1 (left) and line 3 (right)

An estimation of line tensions PSD along the whole line is also provided by the FD model. Figure 17 shows the standard deviation (vertical lines) with respect to the mean tension computed with the analytic catenary equations, along the line. The mean tension difference between both models has been observed to be lower than 1%. In Figure 17 standard deviation differences have been found to be of 1.9% in the fairlead increased

up to 27% in the anchor for lines 1 and 2 and of 8% in the fairlead up to 22% in the anchor for the line 3. Therefore, the FD solution tends to improve line tension estimates as the analysed section is closer to the fairlead with the selected sea state.

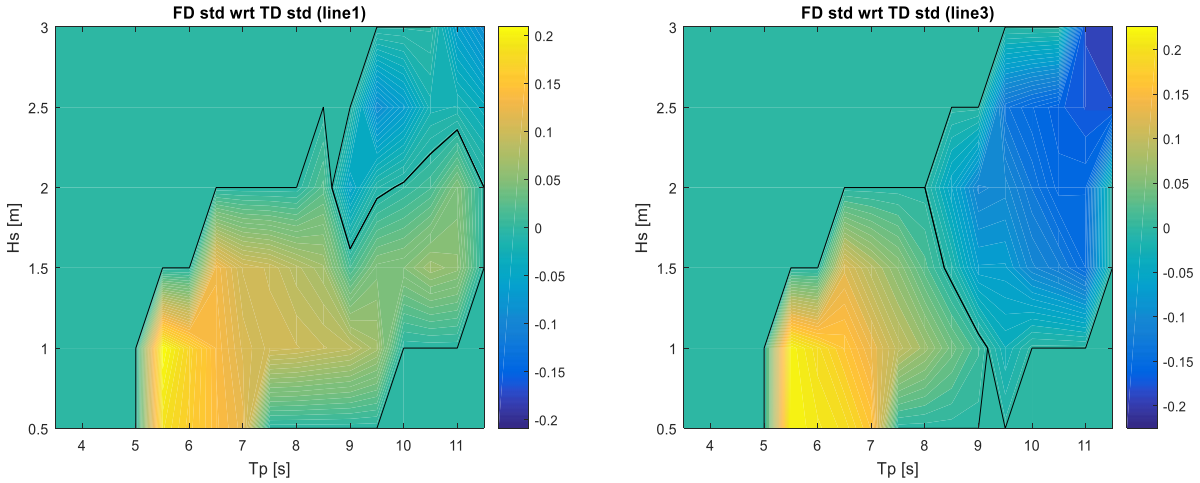

Figure 18. Difference percentage of the linearized FD model with respect to the non-linear TD model in terms of line tensions standard deviation at the fairlead. Contour lines represent zero levels, showing both limits of the selected simulation sea states and limits between under and overestimations of the FD model. Line1: left, Line 3: right.

There is however a remarkable difference between lines tensions obtained with both models in frequencies within 1.3-1.7rad/s, mostly notable in low Hs. The frequency range is coincident with the modes described in Figure 12, as analysed in section 4.1 through the modal analysis. When the device is subject to low Hs sea states, line tension standard deviation values are overestimated with the FD model as shown in Figure 18, as a consequence of the WF range, observed in the PSDs in Figure 19 (top). Good agreement has been obtained for all lines with the device subject to intermediate Hs, especially for the windward lines in the WF range, whilst slightly underestimated in LF for all lines, see Figure 19 c) and d). When analysed in moderate sea states, the windward lines results are improved with respect to lower Hs with some underestimation in the LF range. Nevertheless, Line 3, the leeward line, shows higher differences under moderate Hs, with lines tension standard deviation underestimated up to a 20%, mostly due to the WF range, see Figure 19 f).

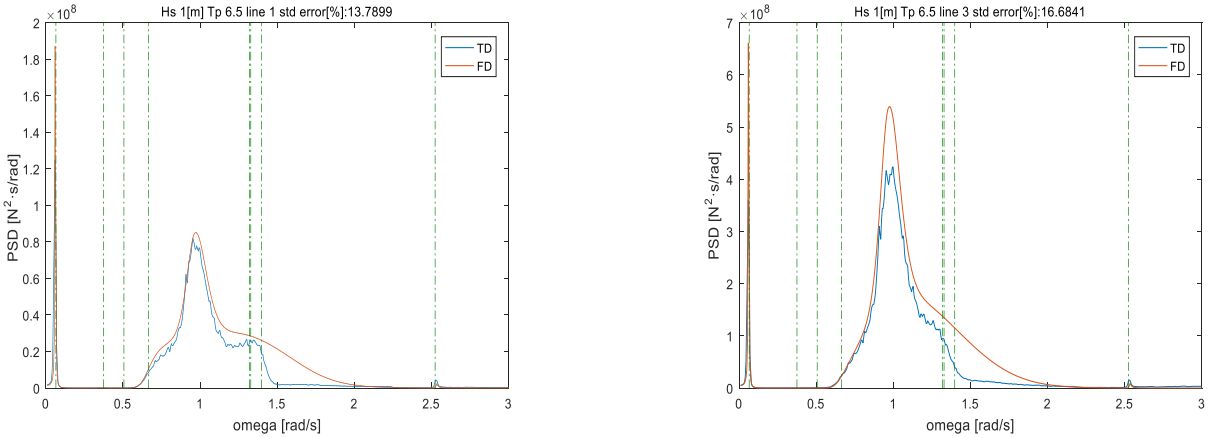

a) b)

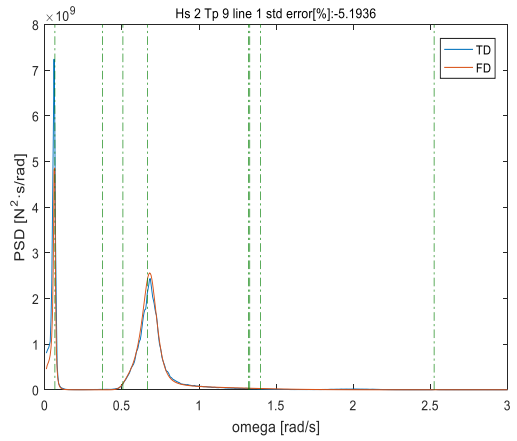

c)

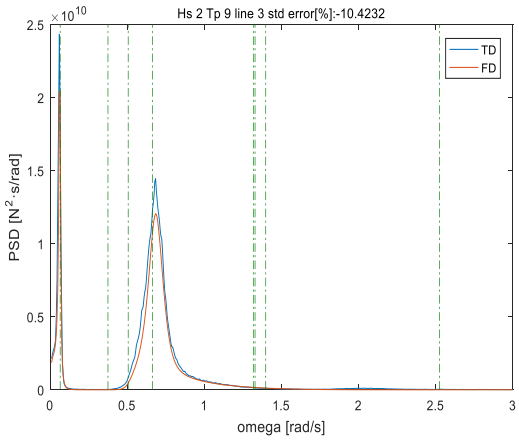

d)

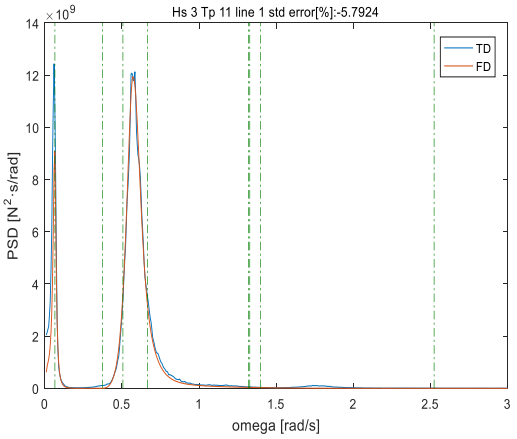

e)

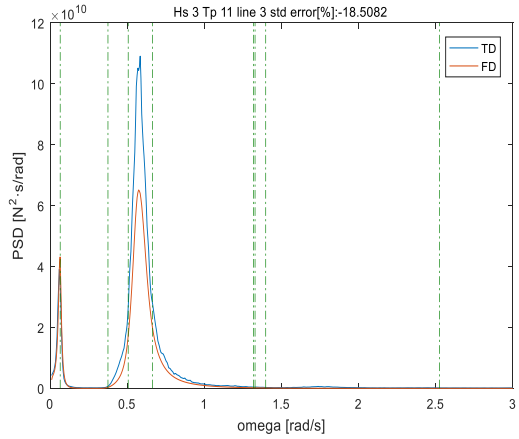

f)

Figure 19. Line tension PSD comparison between the FD and TD models for low Hs, line 1: a) and line 3: b); intermediate Hs, line 1: c) and line 3: d); moderate Hs, line 1: e) and line 3: f). Dash-dotted vertical lines indicate the relevant modes identified in section 4.1

4.4 Discussion

The solution of the linearized FD model has been compared with the non-linear TD in terms of device motions and line tensions. It has been observed that floater dynamics compare significantly well between both models, especially in heave and pitch of both the floating structure and the internal surface water level showing difference percentages lower than 6%. Even though surge also shows good agreement, its results show larger differences, underestimated in up to 20% in standard deviation in sea states with low significant wave heights and low peak periods. These differences can be attributed mainly to deviations on the mooring induced damping.

Resulting line tensions have also been compared between models. The differences have been found to be of the order of those showed by the surge motion, and following similar tendencies, what could be expected as the mooring system is the only source of stiffness in surge. In addition, the linearized model has been found to overestimate line tension PSDs in the frequency range 1.3-1.7[rad/s], coincident with a mode of motion that induces mooring lines' stretching. It is more significant when subject to low Hs sea states and, on the other hand, tensions in the WF range are underestimated when subject to moderate Hs sea states for the leeward line. The underestimation related with the modes of motion showed in Figure 12 can be mostly attributed to non-linear effects caught in the TD model, such as seabed interaction or line sections lifting from the seabed

that the FD model cannot appropriately represent. This effect is limited to low Hs sea states as with higher Hs the excitation induced by the heave motion is more significant and is concentrated in slightly lower frequencies. The differences have also been analysed along the whole lines of the mooring system in one sea state and better agreement has been found as the analysed section approaches the fairlead, whose differences varies from 27% in the anchor decreased up to 1.9% in the fairlead for lines 1 and 2 and of 22% in the anchor up to 8% in the fairlead for the line 3.

The modal analysis, in addition to being able to reproduce non-linear effects only to a certain extent, demonstrates how floating structure motions excite line dynamics. Specially surge and sway have shown to excite line dynamics which induces larger line motions and tensions, which has also been pointed out as another source of difference in surge. Also, it has been showed that the modes within 1.3-1.7[rad/s] are excited in both models and produce significant line tensions. The ability of the FD model to identify such modes provide invaluable information to the mooring designer in order to shift the corresponding natural frequencies away from the natural frequencies in heave.

Even though some differences have been found between both models, it must be noted that the linearized geometric stiffness, introduced in equation (9), accounting for its effect on both the floating structure and mooring line sections, enables the FD model to catch most of the effects and to reproduce power spectral densities of all motions and line tensions.

5 Conclusions

In this paper a numerical method to analyse in the frequency domain floating structures moored by means of catenary mooring systems has been introduced and verified. It is based on a numerical method, already validated, in the TD that couples floating structures modelled through linear potential theory and a lumped mass model, integrating both models into a single one by means of kinematic restrictions based on Lagrange multipliers. The frequency domain model has therefore been made up after linearization of all non-linear terms present in the TD model, mostly related with viscous forces, seabed interaction, lines' fairleads and anchors as well as the geometric stiffness of the catenary lines.

A floating wave energy converter based on OWC technology has been considered as a case study to verify the linearized model with the corresponding non-linear TD model, subject to the most occurrent sea states in BIMEP and with a representative mean current of 0.5m/s. The power take off system has been modelled through a linear damping coefficient acting between the relative heaving motions of the floating structure and the internal surface water level. Damping values of the PTO have been previously optimised to produce the largest mean power per sea state considering both heaving motions. The mooring system has been assumed to be made up of three catenary lines with a significant line pretension to obtain a significant influence of the geometric stiffness. The non-linear TD model has been subject to a sensitivity analysis and in order to reproduce LF response, 12 1-hour TD simulations have been carried out for each of the 36 environmental conditions.

The comparison shows that both floating structure and internal surface water level shows very good agreement, below 6% difference percentages have been found in relative standard deviations except in surge. Surge motion is underestimated with the FD model by up to 20% specially in very low Hs sea states, and mostly due to deviations in the mooring induced damping, whilst with higher Hs the differences have been found to be lower, about 10%.

Line tensions' PSDs show that the influence of all degrees of freedom of the floating structure is well caught. In addition, differences in standard deviations have been found to be of the order of the surge motion. Modal analysis shows how the influence of a mode of motion related with axial stretching of all lines has significant influence in lines tension and is well matched by the FD model. Some differences have been found mostly due to non-linearities not accurately enough reproduced in the FD model. Nevertheless, the linearization carried out in the herein introduced FD model has demonstrated, with a very dynamic floating structure and a mooring with a large pretension, that it can be used to predict both body motions and line tensions within the operational range.

6 Acknowledgments

This work was funded by Project IT949-16 (Departamento de Educación, Política Lingüística y Cultura, Regional Government of the Basque Country).

7 References

[1] H.J.J. Van den Boom, "Dynamic Behaviour of Mooring Lines," *Behaviour of Offshore Structures, Elsevier Science Publishers B V*, pp. 359–368, 1985.

[2] J. Azcona, D. Palacio, X. Munduate, L. González, and T. A. Nygaard, "Impact of mooring lines dynamics on the fatigue and ultimate loads of three offshore floating wind turbines computed with IEC 61400-3 guideline: Impact of mooring lines dynamics on the fatigue and ultimate loads of three offshore floating wind turbines computed with IEC 61400-3 guideline," *Wind Energ.*, vol. 20, no. 5, pp. 797–813, May 2017, doi: 10.1002/we.2064.

[3] M. Hall and A. Goupee, "Validation of a lumped-mass mooring line model with DeepCwind semisubmersible model test data," *Ocean Engineering*, vol. 104, pp. 590–603, Aug. 2015, doi: 10.1016/j.oceaneng.2015.05.035.

[4] "DNVGL-OS-E301.pdf." Accessed: Oct. 26, 2019. [Online]. Available: https://rules.dnvgl.com/docs/pdf/dnvgl/OS/2015-07/DNVGL-OS-E301.pdf.

[5] I. Touzon, V. Nava, B. de Miguel, and V. Petuya, "A Comparison of Numerical Approaches for the Design of Mooring Systems for Wave Energy Converters," *JMSE*, vol. 8, no. 7, p. 523, Jul. 2020, doi: 10.3390/jmse8070523.

[6] F. Cerveira, N. Fonseca, and R. Pascoal, "Mooring system influence on the efficiency of wave energy converters," *International Journal of Marine Energy*, vol. 3–4, pp. 65–81, Dec. 2013, doi: 10.1016/j.ijome.2013.11.006.

[7] J. Fitzgerald and L. Bergdahl, "Including moorings in the assessment of a generic offshore wave energy converter: A frequency domain approach," *Marine Structures*, vol. 21, no. 1, pp. 23–46, Jan. 2008, doi: 10.1016/j.marstruc.2007.09.004.

[8] K. Larsen and P. C. Sandvik, "Efficient Methods For The Calculation Of Dynamic Mooring Line Tension," presented at the The First ISOPE European Offshore Mechanics Symposium, Aug. 1990.

[9] Y. M. Low and R. S. Langley, "Time and frequency domain coupled analysis of deepwater floating production systems," *Applied Ocean Research*, vol. 28, no. 6, pp. 371–385, Dec. 2006, doi: 10.1016/j.apor.2007.05.002.

[10] Y. M. Low and R. S. Langley, "A hybrid time/frequency domain approach for efficient coupled analysis of vessel/mooring/riser dynamics," *Ocean Engineering*, vol. 35, no. 5–6, pp. 433–446, Apr. 2008, doi: 10.1016/j.oceaneng.2008.01.001.
[11] Z. Ran, M. H. Kim, and W. Zheng, "Coupled Dynamic Analysis of a Moored Spar in Random Waves and Currents (Time-Domain Versus Frequency-Domain Analysis)," *Journal of Offshore Mechanics and Arctic Engineering*, vol. 121, no. 3, pp. 194–200, Aug. 1999, doi: 10.1115/1.2829565.
[12] "Ireland leads the way in ocean energy as SEAI funded wave energy device arrives in Hawaii for testing," *Sustainable Energy Authority Of Ireland*. https://www.seai.ie/news-and-media/ocean-energy-test-device/ (accessed Jun. 06, 2020).
[13] "MARMOK-A-5 Wave Energy Converter | Tethys." https://tethys.pnnl.gov/project-sites/marmok-5-wave-energy-converter (accessed Apr. 06, 2020).
[14] "http://www.corpowerocean.com/technology/." http://www.corpowerocean.com/technology/ (accessed Apr. 09, 2020).
[15] R. P. F. Gomes, J. C. C. Henriques, L. M. C. Gato, and A. F. O. Falcão, "Hydrodynamic optimization of an axisymmetric floating oscillating water column for wave energy conversion," *Renewable Energy*, vol. 44, pp. 328–339, Aug. 2012, doi: 10.1016/j.renene.2012.01.105.
[16] F. X. Correia da Fonseca, R. P. F. Gomes, J. C. C. Henriques, L. M. C. Gato, and A. F. O. Falcão, "Model testing of an oscillating water column spar-buoy wave energy converter isolated and in array: Motions and mooring forces," *Energy*, vol. 112, pp. 1207–1218, Oct. 2016, doi: 10.1016/j.energy.2016.07.007.
[17] "ANSYS Aqwa | Hydrodynamics Simulation & Diffraction Analysis." https://www.ansys.com/products/structures/ansys-aqwa (accessed Oct. 27, 2019).
[18] I. Touzon, V. Nava, Z. Gao, I. Mendikoa, and V. Petuya, "Small scale experimental validation of a numerical model of the HarshLab2.0 floating platform coupled with a non-linear lumped mass catenary mooring system," *Ocean Engineering*, vol. 200, p. 107036, Mar. 2020, doi: 10.1016/j.oceaneng.2020.107036.
[19] "BiMEP." https://bimep.com/ (accessed Oct. 26, 2019).
[20] J N Newman, *Marine Hydrodynamics*. U.S.A.: The MIT Press, 2017.
[21] J. Garcia De Jalon, *Kinematic and dynamic simulation of multibody systems: the realtime challenge.* U.S.A.: Springer, 1994.
[22] G. Stipcich, A. Ramezani, V. Nava, I. Touzon, M. Sanchez, and L. Remaki, "Numerical Investigation of the Aerodynamic Performance for a Wells-type Turbine in a Wave Energy Converter," in *MARINE 2015 - Computational Methods in Marine Engineering VI*, Rome, Italy, Jun. 2015, pp. 802–813.
[23] Wendt *et al.*, "Ocean Energy Systems Wave Energy Modelling Task: Modelling, Verification and Validation of Wave Energy Converters," *JMSE*, vol. 7, no. 11, p. 379, Oct. 2019, doi: 10.3390/jmse7110379.
[24] O.M. Faltinsen, *Sea loads on ships and offshore structures*. Cambridge University press, 1990.
[25] J. M. J. J. W.W. Massie, *OffshoreHydromechanics.pdf*, First Edition. Delft: Delft University of Technology, 2001.
[26] I. Touzon, B. de Miguel, V. Nava, V. Petuya, I. Mendikoa, and F. Boscolo, "Mooring System Design Approach: A Case Study for MARMOK-A Floating OWC Wave Energy Converter," in *Volume 10: Ocean Renewable Energy*, Madrid, Spain, Jun. 2018, p. V010T09A025, doi: 10.1115/OMAE2018-77634.
[27] J. A. Pinkster, "Mean and low frequency wave drifting forces on floating structures," *Ocean Engineering*, vol. 6, no. 6, pp. 593–615, Jan. 1979, doi: 10.1016/0029-8018(79)90010-6.
[28] A. F. O. Falcão and L. M. C. Gato, "Air Turbines," in *Comprehensive Renewable Energy*, Elsevier, 2012, pp. 111–149.
[29] A. F. O. Falcão, L. M. C. Gato, and E. P. A. S. Nunes, "A novel radial self-rectifying air turbine for use in wave energy converters," *Renewable Energy*, vol. 50, pp. 289–298, Feb. 2013, doi: 10.1016/j.renene.2012.06.050.
[30] A. F. O. Falcão and J. C. C. Henriques, "The Spring-Like Air Compressibility Effect in OWC Wave Energy Converters: Hydro-, Thermo- and Aerodynamic Analyses," presented at the ASME 2018 37th International Conference on Ocean, Offshore and Arctic Engineering, Sep. 2018, doi: 10.1115/OMAE2018-77096.
[31] "DNV-RP-C205: Environmental Conditions and Environmental Loads," p. 124, 2010.

[32] “MATLAB - El lenguaje del cálculo técnico - MATLAB & Simulink.” https://es.mathworks.com/products/matlab.html (accessed Jul. 05, 2020).